High-Resolution Seismic Reflection/Refraction Imaging from Interstate 10 to Cherry Valley Boulevard, Cherry Valley, Riverside County, California: Implications for Water Resources and Earthquake Hazards

G. Gandhok[1], R. D. Catchings[1], M.R. Goldman[1], E. Horta[1], M. J. Rymer[1], P. Martin[2], and A. Christensen[2]

Open-File Report 99-320

1999

U. S. Geological Survey

[1]Menlo Park, California

[2]San Diego, California

Introduction

This report is the second of two reports on seismic imaging investigations conducted by the U.S. Geological Survey (USGS) during the summers of 1997 and 1998 in the Cherry Valley area in California (Figure 1a). In the first report (Catchings et al., 1999), data and interpretations were presented for four seismic imaging profiles (CV-1, CV-2, CV-3, and CV-4) acquired during the summer of 1997 . In this report, we present data and interpretations for three additional profiles (CV-5, CV-6, and CV-7) acquired during the summer of 1998 and the combined seismic images for all seven profiles. This report addresses both groundwater resources and earthquake hazards in the San Gorgonio Pass area because the shallow (upper few hundred meters) subsurface stratigraphy and structure affect both issues.

The cities of Cherry Valley and Beaumont are located approximately 130 km (~80 miles) east of Los Angeles, California along the southern alluvial fan of the San Bernardino Mountains (Figure 1b). These cities are two of several small cities that are located within San Gorgonio Pass, a lower-lying area between the San Bernardino and the San Jacinto Mountains. Cherry Valley and Beaumont are desert cities with summer daytime temperatures often well above 100° F. High water usage in the arid climate taxes the available groundwater supply in the region, increasing the need for efficient management of the groundwater resources. The USGS and the San Gorgonio Water District (SGWD) work cooperatively to evaluate the quantity and quality of groundwater supply in the San Gorgonio Pass region. To better manage the water supplies within the District during wet and dry periods, the SGWD sought to develop a groundwater recharge program, whereby, excess water would be stored in underground aquifers during wet periods (principally winter months) and retrieved during dry periods (principally summer months). The SGWD preferred a surface recharge approach because it could be less expensive than a recharging program based on injection wells. However, at an existing surface recharge site, surface recharge of the aquifer was limited by the presence of clay-rich layers that impede the downward percolation of the surface water. In boreholes, these clay-rich layers were found to extend from the near surface to about 50 m depth. If practical, the SGWD desired to relocate the recharge ponds to another location within the Cherry Valley–Beaumont area. This required that sites be found where the clay-rich layers were absent. The SGWD elected to explore for such sites by employing a combination of drilling and seismic techniques.

A number of near-surface faults have been suggested in the Cherry Valley-Beaumont area (Figure 1b). However, there may be additional unmapped faults that underlie the alluvial valley of San Gorgonio Pass. Because faults are known to act as barriers to lateral groundwater flow in alluvial groundwater systems, mapped and unmapped subsurface faults in the Cherry Valley-Beaumont area would likely influence groundwater flow and the lateral distribution of recharged water. These same faults may pose a significant hazard to the local desert communities and to greater areas of southern California due to the presence of lifelines (water, electrical, gas, transportation, etc.) that extend through San Gorgonio Pass to larger urban areas.

The three principal goals of the seismic investigation presented in this report were to laterally map the subsurface stratigraphic horizons, locate faults

that may act as barriers to groundwater flow, and measure velocities of shallow sediments that may give rise to amplified shaking during major earthquakes.

Local Geology and Tectonics

The geology within the adjacent San Bernardino Mountains consists largely of pre-Cambrian metamorphic and igneous rocks (gneisses, schists, and Mesozoic granites; Jennings et al., 1977). Within San Gorgonio Pass, Pliocene sandstones, gravels, and clays are overlain by Quaternary alluvium (Jennings et al., 1977). Within the study area, Boyle Engineering Co. (1992) further categorized the upper 300 m of the Quaternary and Pliocene units as the San Timoteo Formation, the Old Red gravel, older alluvium, and recent alluvium. For purposes of discussion in the report, we will use the Boyle Engineering categorization for the shallow-depth lithology.

Along most of the seismic profiles, the upper 20 m of the Quaternary Alluvium unit consists of poorly sorted, unconsolidated gravel, sand, cobbles, and boulders. Underlying the Quaternary alluvium unit is the older alluvium unit, which consists of similar materials that are more consolidated. Beneath the older alluvium unit, the Old Red gravel unit consists of reddish-brown, poorly sorted, coarse gravel, sands, and is about 30 m thick in the Cherry Valley area. The San Timoteo Formation (~75 to 100 m below land surface) is the oldest geologic unit encountered in the boreholes at the existing recharge site, and it consists of poorly sorted to-well-sorted, partly consolidated, fine-to-coarse sand, gravel and cobbles with thin clay layers (Boyle Engineering Co., 1992).

Tectonically, the Cherry Valley-Beaumont area is complex. The study area lies atop an alluvial fan that has been deposited on the southwest side of the San Bernardino Mountains. Major strands of the San Andreas fault trend through the San Bernardino Mountains and within the immediate study area. Strike-slip, thrust, and normal faults have been mapped in the vicinity of our seismic profiles (Figure 1b). Near the northern end of our seismic profiles, the Banning strand of the San Andreas fault has been mapped and consists of both thrust and strike-slip components that vary greatly in strike (Figure 1). Further south along the seismic profile, Matti et al. (1992) infer near-surface faults that are dominantly north-south-oriented and have normal components of motion. This tectonic complexity is caused largely by a change in the strike of the San Andreas fault system from a northwest orientation south of San Gorgonio Pass to one that is predominantly east-west within San Gorgonio Pass.

Seismic Survey

Data Acquisition

In August 1998, the US Geological Survey acquired three high-resolution seismic reflection profiles along Noble Creek in Cherry Valley (Fig 1). These profiles are southward continuations of seismic reflection / refraction profiles acquired further north along Noble and Little San Gorgonio Creeks in July-August, 1997 (Catchings et al., 1999). The seismic profiles acquired in the present study (labeled CV-5, CV-6, and CV-7 in Figure 1a) range in length from about 715 m to about 1609 m (see Table 1). All three profiles had a northeast-southwest orientation.

Approximately 4 s of data were recorded using a linear array with as many as four Geometrics Strataview ™ RX-60 seismographs, each with 60 active channels. The recorded data were stored on the hard drive of the Geometrics Stratiview computers during field acquisition and later downloaded to 4-mm tape for permanent storage in SEG-Y format.

We used 40-Hz, single-element, Mark Products, L-40A™ geophones spaced at 5m intervals along the profiles. Seismic sources (shots), located at depths of about 0.5 m, were laterally spaced approximately every 5 m and were co-located (1m lateral offset) with the geophones along the profiles. The shots were generated by a BETSY Seisgun™ using 8-gauge shotgun blanks. Shot timing was determined electronically at the seismic source when the hammer electrically closed contact with the seisgun, sending an electrical signal to the seismograph.

Prior to acquiring the data, each recording site and shot point was measured with a meter tape and flagged to obtain the proper spacing. After the seismic data were acquired, we used differential Global Positioning System (GPS) measurements to locate recording sites and shot points with a theoretical accuracy of approximately 0.0001 m (see Appendices A, B, and C).

Shot and Geophone Locations

Variations in shot and geophone locations and elevations can cause appreciable difficulty in stacking the reflection data and in accurately measuring the velocities if these variations are not known and considered in processing the seismic data. Large variations in the geometry of the shot and geophone arrays may also result in artifacts in the data that are interpreted as structure. Therefore, we present the line geometries (see Appendices A-C) for those who may wish to reprocess these data. To correlate variations in seismic velocities and seismic image anomalies with possible geometrical variations, we present graphical displays of the geometry along each profile, including shot point and geophone elevations, lateral variations from straight lines of shot point and geophone arrays, and fold. In many instances, abrupt changes in elevation can be correlated with apparent faults or major changes in stratigraphy on the seismic record, but apparent faults or stratigraphic changes that correlate with significant or abrupt changes in shot point and geophone geometry are likely to be artifacts of geometry. Areas with abrupt changes in fold may also contribute to the appearance of artifacts in the seismic data.

Table 1. Acquisition parameters for Cherry Valley seismic profiles. Distances are relative to the first shot point.

Profile #	Orientation	Length of Geophone Profile (m)	Length of Shot Point Profile (m)	# of Shots	# of CDPs	Max Fold
CV-5	NE-SW	715	715	143	286	143
CV-6	NE-SW	964	964	170	340	98
CV-7	NE-SW	1609	1609	317	646	119

Seismic Data Processing

Both reflection and refraction data were available because we used a shoot-through configuration in acquiring the data. This type of data acquisition has numerous advantages over conventional data acquisition because detailed velocity data are available and folds are typically much greater. Detailed velocity data allow for better stacks in the shallow subsurface and also allow depths to be correctly calculated. The shoot-through acquisition method also allows for shallower imaging than is typically afforded in high-resolution seismology (Catchings et al., 1998).

Seismic Refraction Velocity Analysis

We used two types of seismic data processing, refraction analysis and reflection processing. In refraction data processing, we used a seismic tomographic inversion method developed by Hole (1992), whereby, first arrivals on each seismic trace were used to measure detailed velocities for depths ranging from about 1 m below ground surface (bgs) to 250 m (~820 ft) bgs. For greater depths, velocities needed in seismic reflection stacking were determined using semblance and / or parabolic methods and apriori knowledge of the local geology. As described below, we used the velocities derived from these methods to convert the reflection time-images to depth-images and, where necessary, to migrate the seismic reflection images.

Seismic Reflection Processing

Seismic reflection data processing was accomplished on a Sun Sparc 20™ computer using an interactive seismic processing package known as ProMax™. The following steps were involved in data processing:

Geometry Installation

Lateral distances and elevations described above were used to define the geometrical set up of each profile. We installed the GPS-determined geometries (locations) into the ProMax™ processing package for each profile separately so that shot and receiver elevations and locations could be accounted for in the processing routine.

Trace Editing

Occasionally, bad coupling between the geophones and the ground, malfunctioning geophones, or cultural noises close to the seismic receivers resulted in unusually noisy traces at those locations. Traces representing those locations were edited. However, such traces were not always unsuitable for each shot gather; therefore, independent trace editing was employed for each shot gather.

Timing Corrections

Although the shotgun source electronically triggers the seismographs, there are small (~2 ms) delays between the electrical trigger and the actual shotgun explosions. We corrected for the delays by removing a constant 2 ms from the start time of each shot gather. At least two geophones (channels) were overlapped where individual seismograph systems joined. Any relative time variations among seismographs were removed by autocorrelating seismic traces at each overlap.

Elevation Statics

Elevation statics were also employed to correct for variations in elevations along the seismic profile. Velocities needed to make the corrections at each location were determined using the inversion methods described above.

Muting

To remove refractions and other arrivals that were not completely removed using filtering techniques, we used trace muting before and after stacking.

Bandpass Filtering

Most of the data of interest for seismic imaging and velocity measurement are well above 30 Hz, and most of the undesirable seismic data, such as surface waves and shear waves, were well below 30 Hz. Therefore, a bandpass filter with a low cut of 30 Hz was used to remove most surface and shear waves and cultural noise. Post-stack bandpasses were 10-20-200-400.

Gain Correction

An Automatic Gain Control value of 100 ms was added to the data.

F-K Filtering

Not all surface waves were removed by simple bandpass filtering. To remove surface waves and air waves that were not removed by bandpass filtering, we used F-K filtering, which filters on the basis of both frequency and velocity of the arrivals.

Velocity Inversion

As described above, velocities were measured from the seismic data using a computerized inversion routine.

Velocity Analysis

Velocities in the shallow section (~1 m to ~250 m; ~3 to 820 ft) were determined using velocity inversion techniques, but velocities in the deeper section were determined using semblence methods on CDP stacks.

Normal Moveout Correction

Channels that were progressively further from the seismic source experienced a progressively greater delay in the arrival of the seismic signal. To stack the seismic signal, this progressive delay was removed.

Stacking

To increase the strength of the seismic signal and to reduce the strength of random noises, we stacked the signal for each shot.

Depth Conversion

For stacked seismic reflection sections that were not migrated, we converted the time sections to depth sections using RMS velocities converted from the velocity analysis described above in the velocity section.

Migration

Due to the presence of numerous faults and diffraction points in the subsurface, diffraction hyperbolae were observed throughout the sections. We used pre-stack migration to collapse the diffraction hyperbolae to better identify the major faults and structures on depth sections.

Seismic Data

Profile CV-5

Profile CV-5 extended from Woodland Avenue to the intersection of Beaumont Avenue and Noble Creek (Fig. 1a). We used three RX-60 seismographs with 144 live channels to record approximately 143 shots along the

profile. Due to cultural features (gas lines, roads, etc.), one shot point was not utilized. Geophone elevations decreased by about 25 m from northeast to southwest (Fig. 2), and their locations varied from a straight line connecting the endpoints by less than 1 m over approximately 750 m of the array (Fig.3). Similarly, most shot point elevations decreased by less than 25 m from northeast to southwest (Fig. 4), and their locations varied by less than 1 m from a straight-line array (Fig. 5). The minor variation in the linearity of the geophone and shot point arrays suggest that line geometry is unlikely to cause artifacts in the data that can be confused with structure.

Fold along the line varied linearly due to the stationary recording array. Maximum folds of approximately 143 were obtained near the center of the array but decreased to approximately 1 near the ends of the recording array (Fig. 6). This variation in fold suggests that the most reliable reflection image occurs near the center of the array. In practice, however, we've found that folds above about 30 are highly reliable for depths up to about 400 m (~1300 ft) in most areas in California. Thus, for the depths of interest to this investigation, we suggest that the seismic images are likely to be reliable across the entire profile.

Seismic Reflection Images Along Profile CV-5

Stacked and migrated seismic reflection images to depths of approximately 200 m (~650 ft) along profile CV-5 are shown in figure 7. These data show numerous reflections from the near surface to a depth of 200 m bgs. Clear primary reflections are evident in the upper 120 to 160 m, below which, there may be reverberations. Test Well 1 was located within 10 m of the profile CV-5, thereby allowing principal reflections to be correlated with major lithologic units identified in the borehole (Fig. 7). The upper ~60 m correlate with the alluvial layers described by Boyle Engineering (1992), and they appear to be laterally continuous across the profile. Reflections corresponding to the Old Red gravel extend from about 60 m bgs to about 100 m bgs. Below about 100 m, the seismic signal becomes more reverberative within the San Timoteo Formation, as is frequently observed at the transition between sediments to harder rock.

The cumulative sedimentary section shows consistent vertical offsets of layers at several locations along the seismic profile, suggesting that the layers are faulted. Offsets at about meters 500 to 550, meters 350 to 400, and 200 to 250 are observed from the near-surface to depths of about 100 m.

Velocity Section Along Profile CV-5

Seismic velocities along profile CV-5 range from about 400 m/s near the surface to about 2200 m/s at depths of about 200 m (~650 ft) (Fig. 8). Velocities ranging from about 400 m/s to about 1300 m/s correlate with the alluvial layers, and those from about 1400 m/s to about 2100 m/s correlate with the Old Red gravel. Velocities above 2100 m/s correlate with the San Timoteo Formation. The velocity data suggest a thickening of the alluvial units from the northeast to the southwest by nearly 100 percent along profile CV-5. The greatest thickening occurs southwest of meter 500, where a near-vertical velocity anomaly suggests a probable fault.

In unconsolidated alluvial environments, velocities of about 1500 m/s and higher correlate with saturated sediments (Schon, 1996), and velocities below

about 1500 m/s correlate with unsaturated sediments. This correlation between velocity and saturated sediments can be used to infer the water table if the water table is thick enough to propagate seismic waves. On the velocity section (Fig. 8), the 1500 m/s contour (shown in blue) suggests that a water table (perched or otherwise) is located within the upper part of the Old Red gravel.

Combined Velocity and Reflection Images

The seismic velocity inversion model has been superimposed on the seismic reflection images for profile CV-5 (Fig. 9). Seismic reflection images are available for greater depths, but the combined velocity and reflection images show that velocity contours can be correlated with laterally continuous reflections and stratigraphic units identified from borehole logs. This combined image also aids in identifying lateral variations in stratigraphic units because the more consolidated units generally have higher velocities.

Profile CV-6

Profile CV-6 originated near the intersection of Beaumont Avenue and Noble Creek and extended about 900 m southwestward (Fig. 1). We used three RX-60 seismographs with 180 live channels to record approximately 170 shots along the profile. Due to cultural features (gas lines, roads, etc.), 24 shot points were not utilized. Although data were recorded beneath the bridge at Beaumont Avenue, several consecutive shot points were not utilized because of the presence of a concrete liner within Noble Creek.

Geophone elevations decreased by about 30 m from northeast to southwest (Fig. 10), and their locations varied from a straight line connecting the endpoints by less than 5 m over approximately 964 m of the array (Fig. 11). Similarly, shot point elevations also decreased by about 30 m from northeast to southwest (Fig. 12), and their locations varied from a straight-line array by less than 6 m (Fig. 13). The minor variation in linearity of the geophone and shot-point arrays suggest that the line geometry is unlikely to cause artifacts in the data that can be confused with structure. Fold along the profile varied linearly due to the stationary recording array. Maximum folds of approximately 98 were obtained near the center of the array but decreased to approximately one near the ends of the recording array (Fig. 14), suggesting that the best-resolved images are near the center of the array.

Seismic Reflection Images along profile CV-6

Stacked and migrated seismic reflection images to depths of approximately 200 m (~650 ft) along profile CV-6 are shown in figure 15. The northeasternmost end of profile CV-6 overlapped the southwesternmost end of CV-5 by approximately 10 m. These data also show numerous reflections from the near surface to 200 m, with clear primary reflections in the upper 120 to 140 m along most of the profile. However, more coherent and deeper reflections are apparent near the southwestern end of the profile.

Velocity Section along Profile CV-6

The southwestern part of the profile CV-6 overlaps the northeastern part of CV-7 and extends 55 m southwest of the intersection of the two lines. Seismic velocities along profile CV-6 range from about 300 m/s near the surface to about

2400 m/s at depths of about 200 m (~650 ft) (Fig. 16). Velocities ranging from about 400 m/s to about 1300 m/s correlate with the alluvial layers, and those from about 1400 m/s to about 2000 m/s correlate with the Old Red gravel. Velocities above 2000 m/s correlate with the San Timoteo Formation. Unlike profile CV-5, the velocity data do not indicate much southwest thickening of the alluvial units along profile CV-6, which appear to be about 150 m thick. Velocity anomalies between meters 500 and 800 suggest vertical displacement of all units from the San Timoteo to the near-surface alluvial units.

The 1500 m/s velocity contour (blue), which we believe to correlate with the water table, also shows lateral offset near meters 500 and 800. Such a lateral variation in the depth to water table would be expected if the apparent faults inhibit lateral groundwater flow. However, along the southwestern 600 m of the profile, there appears to be little southwestward dip associated with the 1500 m contour.

Combined Velocity and Reflection Images along profile CV-6

The seismic velocity inversion model has been superimposed on the seismic reflection image for profile CV-6 (Fig. 17). The combined image shows the difference in reflection character between the alluvial (blue and green) strata and the more consolidated (yellow and red) strata. In general, the alluvial strata appears to be more laterally continuous.

Wells were not located along profile CV-6, but stratigraphic units can be correlated with those from profiles CV-5 and CV-7, both of which are located near wells with lithologic descriptions (Fig. 17). The upper ~100 m correlate with the alluvial layers, which appear to be largely sub-horizontal (with a slight southwestward dip) and are continuous along profile CV-6. Reflections corresponding to the Old Red gravel extend from about 100 m to about 150 m bgs. Reflections corresponding to the San Timoteo Formation are evident from about 150 to 200 m bgs and appear to be thicker and more coherent. The cumulative sedimentary section shows consistent vertical offsets of layers at several locations along the seismic profile, suggesting that the layers are faulted. Offsets at about meters 850, 725, and 575 respectively, are evident from the near surface to the bottom of the section.

Profile CV-7

Profile CV-7 extended 30 m beyond (overlapped) the southwestern end of profile CV-6. The profiles were processed as two separate profiles because a distinct bend in Noble Creek resulted in appreciably different orientations of the two profiles. Profile CV-7 extended from its intersection with profile CV-6 to a second bend in Noble Creek near the I-10 freeway, a distance of approximately 1600 m. We used three RX-60 seismographs with 180 live channels to record approximately 317 shots along the profile. Due to cultural features (gas lines, roads, etc.), six shot points were not utilized. Geophone elevations decreased by about 37 m from northeast to southwest (Fig. 18), and their locations varied from a straight line connecting the endpoints by less than 7 m over approximately 1609 m of the array (Fig. 19). Similarly, most shot point elevations varied by less than 37 m from northeast to southwest (Fig. 20), and their locations varied by less

than 6 m from a straight-line array (Fig. 21). The minor variation in linearity of the geophone and shot point arrays suggest that line geometry is unlikely to cause artifacts in the data that can be confused with structure. Fold along the profile varied linearly due to the stationary recording array (Fig. 22). Maximum folds of approximately 119 were obtained near the center of the array but decreased to approximately one near the ends of the recording array. This variation in fold suggests that the reflection images are most reliable near the center of the profile.

Seismic Reflection Images along profile CV-7

Stacked and migrated seismic reflection images to depths of approximately 250 m (~820 ft) along profile CV-7 are shown in figure 23. These data show numerous reflections from the near surface to the bottom of the section, with clear primary reflections in the upper ~150 m. The reflection section appears reverberative in the bottom 100 m, but we are not sure whether they are primary reflections or multiples. Because the reflections are not evenly spaced either laterally or vertically, we suggest that most of the reflections are probably not reverberations.

A borehole, with lithologic logs, was located about 100 m west of meter 600 of the profile CV-7. Information from this borehole permits a rough correlation between known stratigraphy and the seismic image. The seismic reflection image shows that the alluvium units are thickest in the northwestern part of the profile, where they are over 100 m thick. These alluvium layers gradually thin to the southwest, where they are about 75 m thick near the end of the profile. On the basis of the reflection data alone, it is not possible to determine the thickness of the Old Red gravel and the San Timoteo Formation, but the reflection data indicate that these more consolidated units do not have appreciable dip to the southwest along profile CV-7. The seismic reflection images show evidence of vertical-offset faulting along most of the profile.

Velocity Section along Profile CV-7

Seismic velocities along profile CV-7 range from about 300 m/s near the surface to about 5000 m/s along an apparent horst structure near meter 600 of the seismic profile (Fig. 24). Along most of the profile, however, maximum velocities were slightly in excess of 4000 m/s at depths of about 250 m (820 ft). Velocities ranging from about 300 m/s to about 1300 m/s correlate with the alluvial layers, and those from about 1400 m/s to 2000 m/s correlate with the Old Red gravel. Velocities ranging from 2000 m/s to 3000 m/s probably correlate with the San Timoteo Formation, but velocities of about 4000 m/s and greater likely correspond to crystalline rocks.

The velocity data suggest thinning of the alluvial units from the northeast to the southwest by nearly 25% along profile CV-7. The thinning appears to be gradual, whereby, less alluvium was deposited on top of the underlying sedimentary and crystalline rocks. A series of horsts and graben are suggested by velocity contours that abruptly rise and fall along the section. These variations in the velocity contours extend to the near surface, suggesting that faults associated with basement horsts and graben extend to the near surface. Maximum vertical relief on the apparent horst and graben structures ranges from about 25 to 50 m.

The 1500 m/s contour (shown in blue) is consistent with the depth of the water table that was measured in the nearby well to the west. The 1500 m/s contour, which we suggest correlates with the water table, rises and falls by about 10 to 20 m over the horst and graben structures, suggesting that the faults associated with these structures act as barriers to lateral flow of groundwater.

Combined Velocity and Reflection Images along profile CV-7

The same general correlation between velocity and reflective character as found along the other two profiles is evident along profile CV-7. However, the combined seismic velocity and reflection image along CV-7 gives a more continuous and clearer image to greater depths (Fig. 25). In general, the alluvial layers have velocities less than 1300 m/s, the Old Red gravel varies in velocity between 1300m/s and 2000 m/s, and the San Timoteo Formation has velocities between 2000m/s and 3000 m/s. The reflection data and the velocity data suggest that these layers vary appreciably and consistently in depth. The vertical variation in depth of the alluvial layers above the horst and graben structures suggest that these faults were active during deposition of the alluvial layers.

Interpretation

Combined Profiles

Structural variation in the upper few hundred meters between Woodland Avenue and the I-10 freeway are most apparent when viewing a composite image of all seismic profiles (Fig. 26 and Fig. 27). The composite data show that the deeper units, principally the Old Red gravel and the San Timoteo Formation have steep dips along profile CV-5. The San Timoteo Fm, in particular, appears to be vertically offset by as much as 100 m along profile CV-5, with the downthrown side on the southwest. The offset represents the largest vertical offset in strata observed along any of the seven profiles acquired in the Cherry Valley–Beaumont area. Both the reflections and the velocity contours representing the San Timoteo Formation dip sharply to the southwest, whereas, the reflections and the velocity contours representing the Quaternary alluvium dip only moderately. The gradient in surface topography as well as the Quaternary alluvium layers is greatest along profile CV-5. These alluvial layers extend into profile CV-6 and are consistent with the dip of the deeper layers. The near-surface alluvial layers thicken by nearly 100 percent along profile CV-5, with a maximum thickness of nearly 150 m. Southwest of this area of apparent faulting, the Old Red gravel and San Timoteo Formation are nearly horizontal except where they are locally faulted.

Summary and Conclusions

The towns of Cherry Valley and Beaumont are located on alluvial fans of the southwestern San Bernardino Mountains. The stratigraphic sequences deposited here are somewhat typical of those deposited along alluvial fans, largely consisting of sand, gravel, clay, and boulders. In the Cherry Valley area, the upper 50 m consist of clay-rich deposits that likely extend along all the profiles (CV-1 through CV-7) from the existing surface recharge ponds in Cherry Valley to near the I-10 freeway. Along the northeasternmost seismic profiles (CV-1 and CV-3), the clay-rich Quaternary Alluvium deposits are only about 50 m thick but appear to thicken at several locations along apparent faults.

Northeast of Woodland Avenue, these layers appear to be no thicker than about 75 m, but southwest of Woodland Avenue, the clay-rich layers rapidly increase to a maximum thickness of about 150 m along a major fault structure. The Quaternary alluvial layers thin from about 150 m at Brookside Ave to about 80 m near the southwestern end of profile CV-7. Although we do not know if these clay-rich layers exist in northwest or southeast of the seismic profiles, deposits in the Noble Creek and Little San Gorgonio Creek drainage basins are probably not significantly different from the rest of the alluvial fan deposits. Thus, it is likely that surface recharge of the groundwater aquifer will be difficult at most locations in the Cherry Valley–Beaumont area.

Seismic velocities in water-saturated alluvial deposits are known to have seismic P-wave velocities of about 1500 m/s (Schon, 1996). The detailed velocity images from this study can therefore be used to infer lateral variations in the water table (perched and/or static) when the water table is thick enough to transmit seismic waves. Wells located along profile CV-3 and near profile CV-7 show that the 1500 m/s contour correlates with the water table observed in those wells. The correlation between velocity and the water level in Test Well 1, located near the northeastern end of CV-5, is inconclusive because: (1) The well is located several tens of meters off the seismic profile. (2) The water level identified in the well may be the deeper static water level, not a perched water level that would be first sensed by the seismic data. (3) Velocity information near the northeastern end of the profile, at the depth of the water table, is not available. (4) The northward continuation of the seismic section to the well location was not imaged, and fault complexity in that area probably affects the depth of the water table. Most of the wells, however, show a strong correlation between the 1500 m/s contour and the water level. Using the 1500 m/s contour as a guide to the water table, the velocity data suggest that the water table is closely aligned with the top of the Old Red gravel.

Because of the complex tectonics associated with the San Andreas fault in the San Gorgonio Pass area, it is not surprising that numerous smaller faults are imaged beneath the Quaternary alluvial cover in San Gorgonio Pass. In fact, some of these faults have been inferred by surface geologic mapping (Matti et al., 1992) (Fig. 28). Most of the smaller individual faults have apparent vertical offsets of about 10 m or less, but some appear to be a series of intense faults with cumulative vertical offsets of several tens of meters. Although these faults appear to be smaller faults, many are predominantly strike-slip faults, and because the seismic images only show the apparent vertical offset, the true vertical or horizontal offset is not known.

In addition to the smaller faults, there appear to be two areas (the northern end of profile CV-3 and the northern end of profile CV-5) with apparent vertical offsets between 50 m and 100 m and several areas with apparent vertical offsets of several tens of meters. These larger-offset faults probably represent significant faults that extend for appreciable distances through San Gorgonio Pass. The larger offset faults appear to correlate with significant bends in the drainages along the alluvial fan, suggesting that strike-slip motion has displaced the drainage laterally. Other similar bends can be seen in drainages further to the northwest and southeast, suggesting that the imaged faults have a northwesterly trend. Along profiles CV-6 and CV-7, a series of horsts and graben, with vertical offsets of several tens of meters are apparent in the seismic images. Similar fault

structures have been mapped at the surface by Matti et al. (1992), who refer to these faults as the "Beaumont Plain fault zone." Matti et al. (1992) show these to be a series of NW-SE-oriented, en-echelon faults that are downthrown to the north and traverse late Quaternary alluvial deposits in the vicinity of Beaumont. However, our data show that these structures are more like horst and graben.

Most hazard assessments for the southern California area assume that most of the slip on the San Andreas fault zone occurs on the mapped traces of the fault. However, the number of imaged faults beneath the alluvial deposits of San Gorgonio Pass and their apparent vertical displacements suggest that an appreciable amount of the slip along the San Andreas fault zone at the latitude of San Gorgonio Pass is accommodated by these buried faults. Assessments that account for the slip on faults not visible at the surface would better estimate the overall slip rate and better assess strain accumulation and recurrence intervals.

Hazards related to strong ground motions in the San Gorgonio Pass area should be re-assessed. Lifelines that extend through San Gorgonio Pass to highly populated areas of southern California, including the Los Angeles metropolitan area may be affected by earthquakes on faults beneath San Gorgonio Pass or by regional earthquakes on other faults of the San Andreas fault zone. Low-velocity, unconsolidated sediments are known to amplify seismic waves and result in violent shaking (Borcherdt et al, 1975: Borcherdt and Glasmoyer, 1994). In the Cherry Valley–Beaumont area, low-velocity (Vp = 300 m/s to 1200 m/s), unconsolidated units are as thick as 150 m. Critical lifelines, including the California Aqueduct, electrical power lines, gas lines, and transportation lines (cars, trains), would likely be impacted by large magnitude earthquakes on either the San Andreas or the faults imaged beneath San Gorgonio Pass.

Data Availability

Digital data from this report are available in SEG-Y format (with elevation and timing corrections applied) from R. D. Catchings at the address on the front of this report.

Acknowledgements

We thank Jeff Dingler, Andy Gallardo, Joseph Grow, Jose Rodriguez, and Scott Strohmeier for assistance in acquiring the seismic data. The project was funded by the San Gorgonio Pass Water Agency, and we particularly thank Steve Stockton for his assistance. Data acquisition and analysis was accomplished through cooperative efforts by the U.S. Geological Survey's Geologic and Water Resources Divisions and the San Gorgonio Pass Water Agency.

References

Borcherdt, R. D., J. F. Gibbs, and K. R. Lajoie, 1975, Prediction of maximum earthquake intensity in the San Francisco Bay region, California, for large earthquakes on the San Andreas and Hayward faults, U.S. Geol. Surv. Misc. Field Studies Map MF-709, 11 pp., scale 1:125,000.

Borcherdt, R. D. and G. Glassmoyer, 1994, Influences of local geology on strong and weak ground motions recorded in the San Francisco Bay region and their implications for site-specific building code provisions, in the Loma Prieta,

California Earthquake of October 17, 1989 - Strong Ground Motion, U.S. Geol. Surv. Profess. Pap. 15512-A, 77-109.

Catchings, R. D., E. Horta, M.R. Goldman, M.J. Rymer, and T.R. Burdette, 1998a, High-resolution seismic imaging for environmental and earthquake hazards assessment at the Raychem Site, Menlo Park, California, U.S. Geol. Surv. Open-File Report 98-146, 37 pp.

Catchings, R. D., M. R. Goldman, W. H. K. Lee, M. J. Rymer and D. J. Ponti, 1998b, Faulting Apparently Related to the 1994 Northridge, California, earthquake and possible co-seismic origin of surface cracks in Potrero Canyon, Los Angeles County, California, Bull. Seis. Soc. America, 88, 1379-1391.

Catchings, R.D., G. Gandhok, M.R. Goldman, E. Horta, and M.J. Rymer, P. Martin, A. Christensen, 1999, High resolution seismic reflection / refraction imaging beneath Cherry Valley, Riverside County, California: Implications for water resources and earthquake hazards, U.S. Geol. Surv. Open-File Report 99-26, 58 pp.

Catchings, R.D. and W.H.K. Lee, 1996, Shallow velocity structure and Poisson's ratio at the Tarzana, California strong motion accelerometer site, Bull. Seis. Soc. America, 86, 1704-1713.

Hauksson, E., L. M. Jones, and K. Hutton, 1995, The 1994 Northridge earthquake sequence in California: Seismological and tectonic aspects, J. Geophys. Res., 97, 12,335-12,355.

Hole, J.A, 1992, Nonlinear high-resolution three-dimensional seismic travel time tomography, J. Geophys. Res., v. 97, p. 6553-6562.

Jennings, C.W., R.G. Strand, and T.H. Rogers, 1977, Geologic Map of California: California Geologic Data Map Series, Map No. 2, map scale 1:750,000.

Matti, J.C., D.M. Morton, and B.F. Cox, 1992, The San Andreas fault system in the vicinity of the central Transverse ranges province, southern California, U.S. Geol. Surv. Open-File Report 92-354.

Schon, J. H., 1996, Physical Properties of Rocks: Fundamentals and Principals of Petrophysics, Handbook of Geophysical Exploration, Seismic Exploration vol. 18, Elsevier Science, Inc., Tarrytown, New York.

List of Figures

Figure.13. Shot point variation from a straight line connecting the first and last geophone along profile CV-6.

Figure. 14. Fold as a function of common depth point (cdp) along profile CV-6.

Figure. 15. Stacked and migrated seismic reflection image along profile CV-6. Depth is relative to the topographically lowest geophone along the profile.

Figure. 16. Seismic velocity inversion model along profile CV-6. Depth is relative to the topographically lowest geophone along the profile.

Figure. 17. Stacked and migrated seismic reflection image of the profile CV-6 with the velocity inversion model superimposed. Depth is relative to the topographically lowest shot point along the profile. The 1500 m/s contour (blue) may correlate with the water table.

Figure.18. Geophone elevation along profile CV-7. Elevation is relative to the topographically lowest geophone along the profile.

Figure.19. Geophone variation from a straight line connecting the first and last geophone in profile CV-7.

Figure.20. Variation in Shot point elevation along Profile CV-7. Elevation is relative to the topographically lowest shot point along the line.

Figure.21. Shot point variation from a straight line connecting the first and last shot point along Profile CV-7.

Figure. 22. Fold as a function of common depth point (cdp) along profile CV-7

Figure. 23. Stacked and migrated seismic reflection image along profile CV-7. Depth is relative to the topographically lowest geophone along the profile.

Figure. 24. Seismic velocity inversion model along profile CV-7. Depth is relative to the topographically lowest geophone along profile CV-7.

Figure. 25. Stacked and migrated seismic reflection image along profile CV-7 with velocity inversion model superimposed. Depth is relative to the topographically lowest shot point along the profile. The 1500 m/s contour (blue)apparently correlates with the water table.

Figure. 26a.Composite reflection-velocity images of the profiles CV-1, CV-2, CV-5, CV-6, and CV-7. Alluvial layers are highlighted with yellow. Test Well 1 is shown in its approximate geographical location along the profiles. The stratigraphy of the well is as follows: Yellow = alluvial layers, Red = Old Red gravel, and Green = San Timoteo Fm.

Figure. 26b. Composite reflection-velocity images of profiles CV-3, CV-4, CV-5, CV-6, and CV-7. Alluvial layers are highlighted with yellow. Test Well 1

is shown in its approximate geographical location along the profiles. The stratigraphy of the well is as follows: Yellow = alluvial layers, Red = Old Red gravel, and Green = San Timoteo Fm.

Figure. 27a Composite seismic velocity inversion models along profiles CV-1, CV-2, CV-5, CV-6, and CV-7 with the locations of wells near the seismic profiles. The 1500 m/s contour is show in blue and correlates with the water table in most wells. Faults are inferred by abrupt vertical changes in the velocity contours.

Figure. 27b. Composite seismic velocity inversion models along profiles CV-3, CV-4, CV-5, CV-6, and CV-7 with the locations of wells near the seismic profiles. The 1500 m/s contour is show in blue and correlates with the water table in most wells. Faults are inferred by abrupt vertical changes in the velocity contours.

Figure 28. Map of Cherry Valley showing location of seismic lines 1 through 7 (blue lines) with faults (red) mapped by Matti et al. (1992). The dashed green line is an inferred fault.

Appendix A
Cherry Valley Line 5

FFID	SP#	SP Dist.	SP Elev.	Geo#	Geo. Dist	Geo. Elev.
1001	1	0	0	1	0	0
1002	2	5.1	0.1	2	5.19	0.15
1003	3	9.97	0.22	3	9.98	0.26
1004	4	15.01	0.32	4	15.02	0.34
1005	6	24.99	0.56	5	20.1	0.45
1006	7	29.94	0.66	6	25.04	0.65
1007	8	35.02	0.8	7	30.04	0.74
1008	9	39.98	0.95	8	35.03	0.85
1009	10	44.9	1.08	9	40.02	0.98
1010	11	49.96	1.22	10	45.04	1.13
1011	12	55.01	1.37	11	49.98	1.31
1012	13	59.95	1.53	12	55.07	1.45
1013	14	64.9	1.66	13	60.03	1.57
1014	15	69.93	1.8	14	65.04	1.73
1015	16	75.08	1.93	15	69.96	1.89
1016	17	79.91	2.06	16	75.15	2
1017	18	84.92	2.18	17	79.99	2.14
1018	19	89.89	2.31	18	84.92	2.27
1019	20	94.91	2.48	19	89.92	2.38
1020	21	99.91	2.64	20	94.9	2.56
1021	22	104.96	2.84	21	99.96	2.69
1022	23	109.99	3.03	22	105.01	2.88
1023	24	114.98	3.22	23	110.19	3.12
1024	25	119.91	3.39	24	115.08	3.34
1025	26	124.98	3.56	25	119.85	3.51
1026	27	129.97	3.73	26	124.9	3.67
1027	28	134.82	3.89	27	130.05	3.89
1028	29	139.91	4.05	28	134.84	4.05
1029	30	144.97	4.2	29	139.82	4.22
1030	31	149.92	4.35	30	144.97	4.32
1031	32	154.98	4.49	31	149.95	4.43
1032	33	159.9	4.66	32	154.95	4.6
1033	34	164.94	4.83	33	159.89	4.74
1034	35	169.88	5.02	34	165.01	4.89
1035	36	174.92	5.19	35	169.74	5.08
1036	37	179.85	5.34	36	175	5.31
1037	38	184.92	5.53	37	179.94	5.48
1038	39	189.89	5.7	38	184.99	5.66
1039	40	194.94	5.86	39	189.95	5.81
1040	41	199.91	6.04	40	194.98	5.98
1041	42	204.87	6.23	41	200.01	6.1
1042	43	209.84	6.42	42	204.95	6.3
1043	44	214.92	6.61	43	209.95	6.48
1044	45	219.92	6.81	44	214.88	6.7
1045	46	224.92	7.01	45	219.98	6.89
1046	47	229.91	7.2	46	224.9	7.06
1047	48	234.89	7.4	47	230	7.25
1048	49	239.83	7.61	48	234.89	7.44
1049	50	244.85	7.82	49	239.91	7.72
1050	51	249.86	8	50	244.85	7.92
1051	52	254.84	8.18	51	249.95	8.12
1052	53	259.79	8.36	52	254.86	8.26
1053	54	264.81	8.55	53	259.84	8.45

Appendix A continued

1054	55	269.79	8.75	54	264.79	8.66
1055	56	274.78	9	55	269.83	8.85
1056	57	279.75	9.25	56	274.87	9.15
1057	58	284.82	9.57	57	279.78	9.35
1058	59	289.84	9.85	58	284.83	9.57
1059	60	294.77	10.09	59	289.74	9.8
1060	61	299.85	10.3	60	294.69	10.08
1061	62	304.86	10.5	61	299.97	10.29
1062	63	309.79	10.66	62	304.84	10.48
1063	64	314.9	10.83	63	309.81	10.65
1064	65	319.81	11	64	314.83	10.82
1065	66	324.75	11.19	65	319.84	11
1066	67	329.8	11.36	66	324.81	11.17
1067	68	334.74	11.52	67	329.82	11.37
1068	69	339.77	11.69	68	334.78	11.54
1069	70	344.82	11.87	69	339.82	11.72
1070	71	349.77	12.04	70	344.79	11.88
1071	72	354.72	12.2	71	349.8	12.03
1072	73	359.78	12.4	72	354.81	12.21
1073	74	364.72	12.61	73	359.9	12.41
1074	75	369.77	12.82	74	364.83	12.61
1075	76	374.74	13.04	75	369.76	12.82
1076	77	379.7	13.22	76	374.84	13.05
1077	78	384.68	13.39	77	379.7	13.24
1078	79	389.71	13.59	78	384.62	13.43
1079	80	394.68	13.75	79	389.77	13.62
1080	81	399.76	13.97	80	394.79	13.81
1081	82	404.75	14.16	81	399.72	13.98
1082	83	409.71	14.36	82	404.78	14.16
1083	84	414.79	14.56	83	409.77	14.34
1084	85	419.76	14.74	84	414.79	14.54
1085	86	424.72	14.92	85	419.72	14.72
1086	87	429.78	15.11	86	424.78	14.91
1087	88	434.76	15.3	87	429.81	15.1
1088	89	439.73	15.48	88	434.73	15.28
1089	90	444.7	15.65	89	439.73	15.46
1090	91	449.81	15.83	90	444.82	15.63
1091	92	454.74	16.03	91	449.75	15.82
1092	93	459.73	16.24	92	454.75	16.02
1093	94	464.74	16.44	93	459.78	16.23
1094	95	469.65	16.62	94	464.77	16.43
1095	96	474.67	16.8	95	469.62	16.62
1096	97	479.7	16.98	96	474.59	16.82
1097	98	484.62	17.19	97	479.67	17.02
1098	99	489.69	17.43	98	484.67	17.24
1099	100	494.64	17.61	99	489.67	17.47
1100	101	499.63	17.81	100	494.74	17.68
1101	102	504.62	17.98	101	499.66	17.86
1102	103	509.61	18.14	102	504.63	18.05
1103	104	514.65	18.3	103	509.66	18.22
1104	105	519.68	18.45	104	514.66	18.34
1105	106	524.7	18.64	105	519.62	18.49
1106	107	529.61	18.8	106	524.74	18.66
1107	108	534.61	18.99	107	529.68	18.85
1108	109	539.58	19.17	108	534.61	19.03
1109	110	544.58	19.36	109	539.71	19.2

Appendix A continued

1110	111	549.63	19.54	110	544.69	19.39
1111	112	554.6	19.73	111	549.67	19.57
1112	113	559.58	19.92	112	554.62	19.76
1113	114	564.57	20.09	113	559.59	19.93
1114	115	569.64	20.26	114	564.58	20.12
1115	116	574.66	20.42	115	569.63	20.3
1116	117	579.64	20.6	116	574.69	20.49
1117	118	584.65	20.76	117	579.68	20.66
1118	119	589.59	20.92	118	584.62	20.83
1119	120	594.63	21.08	119	589.57	20.99
1120	121	599.66	21.26	120	594.61	21.14
1121	122	604.69	21.43	121	599.69	21.31
1122	123	609.6	21.58	122	604.68	21.48
1123	124	614.65	21.75	123	609.58	21.64
1124	125	619.61	21.92	124	614.65	21.79
1125	126	624.6	22.09	125	619.64	21.97
1126	127	629.65	22.26	126	624.67	22.13
1127	128	634.69	22.42	127	629.67	22.29
1128	129	639.66	22.58	128	634.65	22.45
1129	130	644.58	22.73	129	639.64	22.6
1130	131	649.56	22.89	130	644.68	22.75
1131	132	654.62	23.04	131	649.63	22.92
1132	133	659.51	23.22	132	654.64	23.07
1133	134	664.57	23.37	133	659.58	23.21
1134	135	669.56	23.54	134	664.7	23.38
1135	136	674.59	23.69	135	669.59	23.54
1136	137	679.62	23.84	136	674.63	23.7
1137	138	684.56	24.01	137	679.63	23.87
1138	139	689.54	24.18	138	684.59	24.04
1139	140	694.59	24.31	139	689.46	24.21
1140	141	699.58	24.49	140	694.68	24.37
1141	142	704.57	24.62	141	699.71	24.52
1142	143	709.57	24.77	142	704.67	24.69
1143	144	714.61	24.95	143	709.6	24.82
				144	714.63	24.96

Note: FFID is the field file identification number. Distance and elevation are in meters. SP refers to shot point. Geo refers to geophone.

Appendix B
Cherry Valley Line 6

FFID	SP#	SP Dist.	SP Elev.	Geo.#	Geo Dist.	Geo. Elev.
1001	76	375	0	1	0	0
1002	77	380.22	0.1	2	5	0
1003	78	385.05	0.21	3	10	0
1004	79	390.01	0.27	4	15	0
1005	80	395	0.38	5	20	0
1006	81	400	0.48	6	25	0
1007	82	404.98	0.62	7	30	0
1008	83	409.83	0.66	8	35	0
1009	84	414.93	0.75	9	40	0
1010	85	420.08	0.83	10	45	0

Appendix B cont.

1011	86	424.97	1.03	11	50	0
1012	87	430.04	1.19	12	55	0
1013	88	434.93	1.39	13	60	0
1014	89	439.78	1.85	14	65	0
1015	90	444.88	1.62	15	70	0
1016	91	449.85	1.76	16	75	0
1017	92	454.94	1.81	17	80	0
1018	93	459.85	2.14	18	85	0
1019	94	464.98	2.24	19	90	0
1020	95	469.89	2.47	20	95	0
1021	96	474.93	2.53	21	100	0
1022	98	484.92	2.82	22	105	0
1023	99	489.85	2.97	23	110	0
1024	100	494.84	3.09	24	115	0
1025	101	499.86	3.07	25	120	0
1026	102	504.89	3.32	26	125	0
1027	103	509.92	3.43	27	130	0
1028	104	514.92	3.52	28	135	0
1029	105	519.84	3.6	29	140	0
1030	106	524.87	3.76	30	145	0
1031	107	529.82	3.91	31	150	0
1032	108	534.91	3.98	32	155	0
1033	109	539.98	4.15	33	160	0
1034	110	544.85	4.33	34	165	0
1035	111	549.96	4.4	35	170	0
1036	112	554.9	4.57	36	175	0
1037	113	559.85	4.77	37	180	0
1038	114	564.87	4.77	38	185	0
1039	115	569.98	4.76	39	190	0
1040	116	574.89	4.79	40	195	0
1041	117	579.95	5.25	41	200	0
1042	118	584.98	5.36	42	205	0
1043	119	589.95	5.14	43	210	0
1044	120	595	5.42	44	215	0
1045	121	599.98	5.61	45	220	0
1046	122	604.91	5.66	46	225	0
1047	123	609.96	6.06	47	230	0
1048	124	614.95	6.12	48	235	0
1049	125	620.02	6.21	49	240	0
1050	126	624.9	6.3	50	245	0
1051	127	629.94	6.42	51	250	0
1052	128	635	6.53	52	255	0
1053	129	639.97	6.55	53	260	0
1054	130	645.03	6.72	54	265	0
1055	131	650.1	6.82	55	270	0
1056	132	654.99	7.02	56	275	0
1057	133	660.06	7.06	57	280	0
1058	134	664.98	7.2	58	285	0
1059	135	669.95	7.2	59	290	0
1060	136	675.01	7.35	60	295	0
1061	137	680.02	7.43	61	300	0
1062	138	685.12	7.72	62	305	0
1063	139	690.16	7.78	63	310	0
1064	140	695	7.86	64	315	0
1065	141	700.04	7.87	65	320	0
1066	142	705.1	8.05	66	325	0

Appendix B cont.

1067	143	710.08	8.07	67	330	0
1068	144	715.04	8.1	68	335	0
1069	145	720.09	8.67	69	340	0
1070	146	725.1	8.8	70	345	0
1071	147	730.06	8.96	71	350	0
1072	148	735.07	9.05	72	355	0
1073	149	740.06	9.17	73	360	0
1074	150	745.66	9.32	74	365	0
1075	151	749.9	9.43	75	370	0
1076	152	755.06	9.53	76	375.42	-0.02
1077	153	760.1	9.64	77	380.22	0.17
1078	154	765.01	9.77	78	385.04	0.26
1079	155	770.14	9.92	79	389.92	0.26
1080	156	775.07	10.06	80	394.89	0.26
1081	157	780.1	10.17	81	399.93	0.49
1082	158	785.15	10.28	82	404.87	0.55
1083	159	790.18	10.41	83	409.93	0.82
1084	160	795.14	10.5	84	414.97	0.9
1085	161	800.14	10.59	85	420.06	0.84
1086	162	805.13	10.71	86	425.04	0.84
1087	163	810.07	10.23	87	429.97	1.19
1088	165	820.14	10.39	88	434.92	1.34
1089	167	830.13	10.68	89	439.79	1.52
1090	168	835.13	10.71	90	444.88	1.58
1091	169	840.14	11.03	91	449.78	1.76
1092	170	845.19	11.32	92	454.84	1.88
1093	171	850.18	11.3	93	459.83	2.1
1094	172	855.22	11.35	94	464.95	2.29
1095	173	860.16	11.53	95	469.93	2.43
1096	174	865.16	11.59	96	474.89	2.55
1097	175	870.15	11.7	97	479.77	2.63
1098	176	875.13	11.81	98	485.01	2.85
1099	177	880.06	11.9	99	489.9	2.85
1100	178	885.06	12.05	100	494.83	3.02
1101	179	890.1	12.17	101	499.85	3.18
1102	180	895.07	12.21	102	505.03	3.17
1103	181	900.11	12.3	103	509.91	3.41
1104	182	905.06	12.45	104	514.99	3.48
1105	183	910.09	12.47	105	520.01	3.58
1106	184	915.05	12.58	106	524.91	3.76
1107	185	920.06	12.62	107	529.89	3.85
1108	186	925.08	13.08	108	534.82	3.98
1109	187	930.01	13.26	109	539.95	4.08
1110	188	935	13.4	110	544.67	4.3
1111	189	940.08	13.56	111	550.01	4.46
1112	190	945.03	13.58	112	554.82	4.53
1113	191	950.06	14.22	113	559.89	4.69
1114	192	955.08	14.72	114	564.87	4.86
1115	193	959.99	15.62	115	570.05	4.75
1116	195	969.75	17.14	116	575.08	4.78
1117	196	974.86	17.26	117	579.8	4.93
1118	197	979.87	17.35	118	584.85	5.02
1119	198	984.79	17.51	119	589.92	5.17
1120	199	989.78	17.56	120	595	5.33
1121	200	994.79	17.68	121	600.03	5.61
1122	201	999.65	17.9	122	604.9	5.71

Appendix B cont.

1123	2021004.72	18.14	123	609.9	5.97
1124	2041014.69	18.35	124	615.01	6.05
1125	2051019.69	18.45	125	619.89	6.17
1126	2061024.85	18.67	126	624.96	6.29
1127	2071029.68	18.82	127	630.03	6.43
1128	2081034.68	19.1	128	634.88	6.52
1129	2091039.67	19.45	129	640.02	6.63
1130	2101044.75	20.01	130	645.12	6.73
1131	2111049.78	20.22	131	649.93	6.86
1132	2121054.64	20.51	132	655.11	6.94
1133	2131059.61	19.87	133	660.08	7.09
1134	2141064.62	19.84	134	664.96	7.19
1135	2171079.64	19.91	135	670.15	7.12
1136	218 1084.8	20.05	136	674.99	7.33
1137	219 1089.8	20.07	137	680.05	7.52
1138	2201094.78	20.24	138	685.2	7.68
1139	2221104.74	20.74	139	690.19	7.75
1140	2231109.58	20.82	140	695.01	7.97
1141	2241114.59	20.94	141	700.11	8.03
1142	2251119.71	21.27	142	705.26	8.02
1143	2261124.88	21.32	143	710.19	8.03
1144	2271129.81	21.39	144	715.18	8.56
1145	2281134.65	21.66	145	720.15	8.65
1146	2291139.64	22.01	146	725.19	8.81
1147	230 1144.7	22.23	147	730.04	8.94
1148	2311149.52	22.52	148	735.15	9.04
1149	2321154.69	22.64	149	740.01	9.18
1150	2331159.68	22.71	150	745.22	9.28
1151	2341164.74	22.91	151	750.16	9.37
1152	2351169.86	22.95	152	755.12	9.48
1153	2361174.65	23.03	153	760.15	9.67
1154	2371179.68	23.46	154	765.1	9.83
1155	238 1184.6	23.54	155	770.16	9.92
1156	2401194.61	23.68	156	775.11	10.04
1157	2411199.68	23.77	157	780.17	10.18
1158	242 1204.6	23.88	158	785.24	10.29
1159	2431209.59	23.9	159	790.12	10.41
1160	2441214.61	24.11	160	795.31	10.48
1161	2451219.56	24.33	161	800.31	10.59
1162	2461224.94	24.53	162	805.25	10.69
1163	2471229.59	24.69	163	810.09	10.83
1164	2481234.58	24.86	164	814.9	10.95
1165	2491239.51	25.05	165	820	10.52
1166	2501244.52	25.24	166	825.24	10.51
1167	2661324.03	29.03	167	830.16	10.82
1168	2671329.12	29.16	168	835.07	10.76
1169	2681334.08	29.28	169	840.01	10.89
1170	2691338.82	29.36	170	845.17	11.06
			171	850.19	11.3
			172	855.16	11.43
			173	860.05	11.45
			174	864.84	11.63
			175	870.01	11.66
			176	875.18	11.77
			177	880.13	11.89
			178	885.16	11.99

Appendix B cont.

179	890.11	12.13
180	895.18	12.25
181	900.08	12.36
182	905.19	12.48
183	910.19	12.54
184	915.04	12.41
185	920.05	12.5
186	925.06	12.6
187	930.05	13.45
188	935.11	13.57
189	940.23	13.65
190	945.05	13.58
191	950.02	14.18
192	955.08	14.53
193	960	15.37
194	964.88	16.79
195	969.73	17.15
196	974.85	17.26
197	979.78	17.37
198	984.7	17.42
199	989.76	17.49
200	994.89	17.6
201	999.62	17.83
202	1004.68	18.02
203	1009.67	18.24
204	1014.52	18.33
205	1019.73	18.44
206	1024.66	18.62
207	1029.63	18.81
208	1034.74	19.05
209	1039.59	19.36
210	1044.78	19.98
211	1049.8	20.23
212	1054.75	20.42
213	1059.84	19.83
214	1064.64	19.75
215	1069.69	19.77
216	1074.74	19.79
217	1079.79	19.81
218	1084.92	20.05
219	1089.87	20.09
220	1095.08	20.28
221	1099.95	20.51
222	1105.04	20.73
223	1109.8	20.85
224	1114.69	21
225	1119.73	21.25
226	1124.75	21.31
227	1129.73	21.37
228	1134.63	21.68
229	1139.87	21.92
230	1144.54	22.18
231	1149.48	22.51
232	1154.52	22.64
233	1159.6	22.76
234	1164.63	23.01

Appendix B cont.

235	1169.85	22.99
236	1174.64	23.04
237	1179.5	23.4
238	1184.58	23.57
239	1189.74	23.61
240	1194.57	23.64
241	1199.68	23.7
242	1204.62	23.76
243	1209.84	23.91
244	1214.62	24.07
245	1219.75	24.29
246	1224.85	24.48
247	1229.73	24.65
248	1234.69	24.81
249	1239.74	24.99
250	1244.46	25.19
251	1249.7	23.78
252	1254.51	23.87
253	1259.52	24.11
254	1264.49	24.36
255	1269.53	24.39
256	1274.69	24.64
257	1279.69	24.84
258	1284.69	25.04
259	1289.69	25.24
260	1294.79	25.44
261	1299.79	25.64
262	1304.89	25.89
263	1309.66	26.1
264	1314.8	28.6
265	1318.92	28.85
266	1323.93	28.98
267	1328.98	29.13
268	1333.94	29.23
269	1338.82	29.36
270	1345	30
271	1350	30
272	1355	30
273	1360	30
274	1365	30
275	1370	30
276	1375	30
277	1380	30
278	1385	30
279	1390	30
280	1395	30
281	1400	30
282	1405	30
283	1410	30
284	1415	30
285	1420	30
286	1425	30
287	1430	30

Note: Distance and elevation are in meters. FFID refers to field file identification number. SP refers to shot point. Geo. refers to geophone.

Appendix C
Cherry Valley Line 7

FFID	SP#	SP Dist.	SP Elev.	Geo#	Geo Dist	Geo Elev.
1001	1	0	0	12	55.08	1.26
1002	2	5.11	0.3	13	60.07	1.41
1003	3	10.17	0.6	14	64.96	1.51
1004	4	15.18	0.66	15	70.06	1.63
1005	5	20.2	0.68	16	75.14	1.72
1006	6	25.08	0.81	17	80.16	1.77
1007	7	30.09	0.89	18	85.06	1.89
1008	8	35.39	1.02	19	90.08	2.05
1009	9	40.25	0.98	20	95.22	2.07
1010	10	45.18	1.08	21	99.98	2.11
1011	11	50.13	1.12	22	105.03	2.25
1012	12	55.08	1.26	23	109.98	2.31
1013	13	60.07	1.41	24	115.07	2.46
1014	14	64.96	1.51	25	120.05	2.52
1015	15	70.06	1.63	26	125.12	2.63
1016	16	75.14	1.72	27	130.06	2.66
1017	17	80.16	1.77	28	134.85	2.72
1018	18	85.06	1.89	29	140.11	2.81
1019	19	90.08	2.05	30	145.16	2.98
1020	20	95.22	2.07	31	150.01	3.05
1021	21	99.98	2.11	32	155.07	3.14
1022	22	105.03	2.25	33	160.03	3.2
1023	23	109.98	2.31	34	164.93	3.31
1024	24	115.07	2.46	35	170.04	3.45
1025	25	120.05	2.52	36	174.95	3.55
1026	26	125.12	2.63	37	180.07	3.7
1027	27	130.06	2.66	38	185.01	3.88
1028	28	134.85	2.72	39	190.17	3.98
1029	29	140.11	2.81	40	195.25	4.06
1030	30	145.16	2.98	41	200.26	4.16
1031	31	150.01	3.05	42	205.19	4.24
1032	32	155.07	3.14	43	210.23	4.29
1033	33	160.03	3.2	44	215.24	4.51
1034	34	164.93	3.31	45	220.21	4.64
1035	35	170.04	3.45	46	225.24	4.71
1036	36	174.95	3.55	47	230.22	4.83
1037	37	180.07	3.7	48	235.24	5.04
1038	38	185.01	3.88	49	240.13	5.18
1039	39	190.17	3.98	50	245.27	5.3
1040	40	195.25	4.06	51	250.26	5.4
1041	41	200.26	4.16	52	255.26	5.46
1042	42	205.19	4.24	53	260.29	5.59
1043	43	210.23	4.29	54	265.27	5.72
1044	44	215.24	4.51	55	270.25	5.82
1045	45	220.21	4.64	56	275.28	5.87
1046	46	225.24	4.71	57	280.23	5.98
1047	47	230.22	4.83	58	285.29	6.06

Appendix C cont.

1048	48	235.24	5.04	59	290.2	6.15
1049	49	240.13	5.18	60	295.28	6.24
1050	50	245.27	5.3	61	300.3	6.34
1051	51	250.26	5.4	62	305.4	6.44
1052	52	255.26	5.46	63	310.5	6.54
1053	53	260.29	5.59	64	315.4	6.64
1054	54	265.27	5.72	65	320.28	6.69
1055	55	270.25	5.82	66	325.33	6.9
1056	56	275.28	5.87	67	330.29	6.95
1057	57	280.23	5.98	68	335.29	7.11
1058	58	285.29	6.06	69	340.37	7.26
1059	59	290.2	6.15	70	345.29	7.39
1060	60	295.28	6.24	71	350.34	7.52
1061	66	325.33	6.9	72	355.43	7.55
1062	67	330.29	6.95	73	360.3	7.79
1063	68	335.29	7.11	74	365.4	7.85
1064	69	340.37	7.26	75	370.31	7.96
1065	70	345.29	7.39	76	375.43	8.1
1066	71	350.17	7.44	77	380.27	8.21
1067	72	355.37	7.48	78	385.35	8.32
1068	73	360.21	7.68	79	390.19	8.42
1069	74	365.24	7.87	80	395.29	8.54
1070	75	370.25	7.91	81	400.11	8.64
1071	76	375.24	8	82	405.27	8.8
1072	77	380.27	8.19	83	410.34	8.84
1073	78	385.2	8.27	84	415.22	8.96
1074	79	390.25	8.45	85	420.21	9.04
1075	80	395.4	8.54	86	425.17	9.22
1076	81	400.35	8.69	87	430.09	9.25
1077	82	405.27	8.76	88	435.1	9.43
1078	83	410.3	8.86	89	440.34	9.52
1079	84	415.15	9.01	90	445.27	9.73
1080	85	420.26	9.03	91	450.2	9.85
1081	86	425.18	9.15	92	455.15	9.95
1082	87	430.31	9.32	93	460.22	10.05
1083	88	435.22	9.41	94	465.36	10.1
1084	89	440.15	9.55	95	470.33	10.19
1085	90	445.15	9.68	96	475.28	10.32
1086	91	450.23	9.8	97	480.16	10.47
1087	92	455.23	9.91	98	485.03	10.61
1088	93	460.1	10.02	99	490.18	10.67
1089	94	465.18	10.21	100	495.19	10.86
1090	95	470.14	10.12	101	500.24	11.05
1091	96	475.11	10.01	102	505.22	11.23
1092	97	480.19	10.43	103	510.22	11.22
1093	98	485.18	10.53	104	515.31	11.34
1094	99	489.95	10.85	105	520.2	11.48
1095	100	495.18	10.77	106	525.02	11.61
1096	101	500.19	10.8	107	530.15	11.72
1097	102	505.25	11.01	108	535.16	11.8
1098	103	510.31	11.14	109	540.2	11.88
1099	104	515.18	11.18	110	545.23	12
1100	105	520.25	11.31	111	550.24	12.16
1101	106	525.29	11.46	112	555.15	12.27
1102	107	530.24	11.7	113	560.43	12.4
1103	108	535.13	11.7	114	565.36	12.5

Appendix C cont.

1104	109	540.17	11.82	115	570.23	12.61
1105	110	545.17	11.94	116	575.22	12.84
1106	111	550.19	12.05	117	580.36	12.91
1107	112	555.14	12.26	118	585.21	13.09
1108	113	560.35	12.33	119	590.27	13.24
1109	114	565.2	12.49	120	595.21	13.32
1110	115	570.2	12.65	121	600.26	13.38
1111	116	575.26	12.68	122	605.18	13.55
1112	117	580.26	12.86	123	610.4	13.64
1113	118	585.21	12.99	124	615.3	13.8
1114	119	590.19	13.16	125	620.33	13.84
1115	120	595.17	13.22	126	625.2	14.01
1116	121	600.23	13.38	127	630.39	14.1
1117	122	605.19	13.5	128	635.17	14.4
1118	123	610.33	13.59	129	640.35	14.31
1119	124	615.3	13.75	130	645.32	14.48
1120	125	620.11	13.83	131	650.35	14.59
1121	126	625.07	13.94	132	655.21	14.68
1122	127	630.18	14.06	133	660.28	14.79
1123	128	635.17	14.15	134	665.25	14.93
1124	129	640.23	14.27	135	670.1	15.06
1125	130	645.23	14.38	136	675.24	15.19
1126	131	650.22	14.5	137	680.13	15.32
1127	132	655.2	14.59	138	685.28	15.5
1128	133	660.26	14.72	139	690.24	15.62
1129	134	665.14	14.85	140	695.23	15.77
1130	135	670.26	14.95	141	700.23	15.85
1131	136	675.19	15.13	142	705.27	15.97
1132	137	680.17	15.18	143	710.25	16.06
1133	138	685.24	15.43	144	715.36	16.12
1134	139	690.21	15.53	145	720.24	16.32
1135	140	695.24	15.65	146	725.08	16.47
1136	141	700.17	15.91	147	730.22	16.6
1137	142	705.3	15.99	148	735.23	16.68
1138	143	710.23	16.06	149	740.11	16.77
1139	144	715.24	16.16	150	745.18	16.91
1140	145	720.38	16.31	151	750.19	17.09
1141	146	725.19	16.44	152	755.28	17.13
1142	147	730.23	16.5	153	760.14	17.35
1143	148	735.21	16.58	154	765.09	17.42
1144	149	740.29	16.73	155	770.13	17.55
1145	150	745.22	16.84	156	775.24	17.63
1146	151	750.22	16.94	157	780.19	17.71
1147	152	755.27	17.11	158	785.18	17.8
1148	153	760.32	17.28	159	790.22	17.86
1149	154	765.24	17.39	160	795.2	18.02
1150	155	770.29	17.45	161	800.11	18.13
1151	156	775.22	17.6	162	805.17	18.24
1152	157	780.2	17.63	163	810.2	18.31
1153	158	785.18	17.78	164	815.15	18.44
1154	159	790.26	17.83	165	820.2	18.57
1155	160	795.24	17.99	166	825.32	18.59
1156	161	800.21	18.11	167	830.21	18.63
1157	162	805.23	18.18	168	835.18	18.82
1158	163	810.35	18.29	169	840.17	19.06
1159	164	815.32	18.42	170	845.25	19.15

Appendix C cont.

1160	165	820.26	18.47	171	850.23	19.17
1161	166	825.17	18.57	172	855.2	19.43
1162	167	830.18	18.7	173	860.2	19.55
1163	168	835.27	18.8	174	865.24	19.69
1164	169	840.24	18.92	175	870.22	19.77
1165	170	845.17	19.02	176	875.37	19.88
1166	171	850.25	19.2	177	880.23	20.03
1167	172	855.19	19.31	178	885.3	20.1
1168	173	860.13	19.5	179	890.2	20.18
1169	174	865.29	19.68	180	895.32	20.5
1170	175	870.22	19.76	181	900.4	20.46
1171	176	875.17	19.85	182	905.43	20.52
1172	177	880.34	20.06	183	910.14	20.57
1173	178	885.2	20.15	184	915.18	20.92
1174	179	890.24	20.17	185	920.31	21.14
1175	180	895.27	20.4	186	925.26	21.16
1176	181	900.28	20.53	187	930.16	21.36
1177	182	905.26	20.63	188	935.1	21.68
1178	183	910.12	20.92	189	940.21	21.74
1179	184	915.12	20.91	190	945.27	21.63
1180	185	920.19	21.15	191	950.29	22.1
1181	186	925.28	21.21	192	955.15	21.88
1182	187	930.27	21.42	193	960.01	21.93
1183	188	935.15	21.31	194	965.17	22.14
1184	189	940.21	21.49	195	970.24	22.06
1185	190	945.29	21.6	196	975.21	22.16
1186	191	950.22	21.92	197	980.26	22.28
1187	192	955.2	22.11	198	985.24	22.48
1188	193	960.15	21.94	199	990.22	22.58
1189	194	965.18	21.97	200	995.3	22.68
1190	195	970.24	22.03	201	1000.29	22.75
1191	196	975.21	22.14	202	1005.34	22.89
1192	197	980.22	22.3	203	1010.27	23.21
1193	198	985.25	22.39	204	1015.31	23.18
1194	199	990.28	22.65	205	1020.31	23.36
1195	200	995.21	22.7	206	1025.29	23.68
1196	201	1000.14	22.75	207	1030.41	24.01
1197	202	1005.18	22.85	208	1035.43	23.94
1198	203	1010.19	23.12	209	1040.57	24.08
1199	204	1015.19	23.29	210	1045.47	24.21
1200	205	1020.22	23.33	211	1050.52	24.31
1201	206	1025.23	23.56	212	1055.33	24.44
1202	207	1030.3	23.79	213	1060.26	24.61
1203	208	1035.26	24.06	214	1065.41	24.72
1204	209	1040.46	24.08	215	1070.38	24.85
1205	210	1045.35	24.19	216	1075.34	24.95
1206	211	1050.29	24.35	217	1080.47	25.04
1207	212	1055.29	24.47	218	1085.22	25.17
1208	213	1060.27	24.62	219	1090.35	25.37
1209	214	1065.36	24.72	220	1095.33	25.55
1210	215	1070.3	24.83	221	1100.44	25.61
1211	216	1075.24	24.88	222	1105.42	25.61
1212	217	1080.19	25.04	223	1110.25	25.74
1213	218	1085.22	25.32	224	1115.29	25.81
1214	219	1090.23	25.34	225	1120.28	25.9
1215	220	1095.26	25.56	226	1125.33	26.04

Appendix C cont.

1216	2211100.31	25.52	227	1130.26	26.19
1217	2221105.43	25.56	228	1135.16	26.29
1218	223 1110.3	25.67	229	1140.24	26.41
1219	224 1115.3	25.8	230	1145.33	26.57
1220	2251120.28	25.94	231	1150.3	26.75
1221	2261125.21	26.09	232	1155.34	26.84
1222	2271130.14	26.17	233	1160.21	26.93
1223	2281135.17	26.3	234	1165.17	27.12
1224	2291140.21	26.41	235	1170.29	27.32
1225	2301145.21	26.56	236	1175.25	27.36
1226	2311150.21	26.71	237	1180.24	27.56
1227	2321155.17	26.81	238	1185.18	27.63
1228	2331160.16	26.91	239	1190.13	27.72
1229	234 1165.1	27.08	240	1195.16	27.86
1230	2351170.23	27.2	241	1200.21	27.99
1231	236 1175.2	27.32	242	1205.09	28.14
1232	2371180.16	27.52	243	1210.05	28.32
1233	2381185.15	27.6	244	1215.12	28.33
1234	2391190.09	27.74	245	1220.12	28.48
1235	2401195.15	27.83	246	1225.12	28.67
1236	2411200.12	27.98	247	1230.22	28.82
1237	2421205.13	28.16	248	1234.75	28.85
1238	2431210.05	28.28	249	1239.81	29.01
1239	2441215.06	28.36	250	1245.05	29.01
1240	2451220.06	28.53	251	1250.06	29.13
1241	2461225.09	28.68	252	1255.12	29.25
1242	247 1230.1	28.76	253	1260	29.41
1243	2481235.03	28.89	254	1265.08	29.54
1244	2491240.08	28.91	255	1270.1	29.65
1245	250 1245.1	29.15	256	1275.22	29.76
1246	2511250.07	29.14	257	1280.05	29.89
1247	2521255.05	29.3	258	1285.12	30.09
1248	2531260.07	29.41	259	1290.16	30.18
1249	2541265.04	29.57	260	1295.15	30.27
1250	2551270.06	29.64	261	1300.16	30.4
1251	2561275.09	29.79	262	1305.17	30.51
1252	2571280.11	29.86	263	1310.11	30.62
1253	2581285.05	30.05	264	1315.03	30.67
1254	2591290.13	30.21	265	1320.05	30.8
1255	2601295.16	30.28	266	1325.09	30.91
1256	2621305.09	30.51	267	1330.23	31.12
1257	263 1310	30.61	268	1335.16	31.28
1258	2641315.02	30.69	269	1340.19	31.4
1259	2651320.06	30.83	270	1345.16	31.48
1260	2661325.06	30.92	271	1350.21	31.66
1261	2671330.14	31.07	272	1355.15	31.78
1262	2681335.07	31.18	273	1360.2	31.83
1263	2691340.04	31.32	274	1365.05	31.94
1264	2701345.12	31.53	275	1370.24	32.05
1265	2711350.22	31.64	276	1375.21	32.18
1266	2721355.06	31.73	277	1380.21	32.34
1267	2731360.08	31.81	278	1385.24	32.47
1268	2741365.07	31.92	279	1390.15	32.57
1269	2751370.09	32.06	280	1395.36	32.69
1270	2761375.14	32.16	281	1400.28	32.85
1271	2771380.14	32.32	282	1405.34	32.95

Appendix C cont.

1272	278 1385.2	32.44	283	1410.2	33.03
1273	2791390.23	32.54	284	1415.12	33.09
1274	280 1395.2	32.73	285	1420.17	33.24
1275	2811400.21	32.85	286	1425.1	33.36
1276	2821405.18	32.94	287	1430.09	33.46
1277	2831410.12	33.02	288	1435.11	33.51
1278	2841415.11	33.14	289	1440.18	33.69
1279	2851420.13	33.22	290	1445.26	33.81
1280	2861425.19	33.33	291	1450.19	33.94
1281	2871430.18	33.42	292	1455.22	34.02
1282	2881435.19	33.5	293	1459.94	34.12
1283	2891440.16	33.72	294	1464.64	34.26
1284	2901445.22	33.78	295	1469.5	34.58
1285	2911450.18	33.93	296	1474.66	34.82
1286	292 1455.2	34	297	1479.57	34.81
1287	293 1459.9	34.13	298	1484.66	34.97
1288	2941464.54	34.33	299	1489.61	35.1
1289	2951469.55	34.44	300	1494.66	35.22
1290	2961474.48	34.59	301	1499.49	35.33
1291	2971479.66	34.7	302	1504.59	35.47
1292	2981484.57	34.95	303	1509.56	35.57
1293	2991489.55	35.07	304	1514.56	35.7
1294	3001494.56	35.18	305	1519.64	35.83
1295	3011499.56	35.35	306	1524.51	35.89
1296	3021504.55	35.44	307	1529.37	36.08
1297	3031509.54	35.57	308	1534.49	36.17
1298	3041514.51	35.63	309	1539.55	36.3
1299	3051519.57	35.79	310	1544.67	36.44
1300	3061524.52	35.88	311	1549.4	36.49
1301	3071529.53	36.08	312	1554.4	36.65
1302	3081534.56	36.22	313	1559.37	36.82
1303	3091539.63	36.34	314	1564.43	36.91
1304	310 1544.6	36.44	315	1569.39	37.14
1305	3111549.52	36.58	316	1574.43	37.17
1306	3121554.56	36.7	317	1579.48	37.12
1307	3131559.43	36.87	318	1584.52	37.47
1308	3141564.44	37.1	319	1589.43	37.58
1309	3151569.46	36.96	320	1594.38	37.74
1310	3161574.52	37.25	321	1599.52	37.98
1311	3171579.49	37.41	322	1604.42	38.02
1312	3181584.56	37.52	323	1609.59	38.03
1313	3191589.45	37.63	324	1615	38
1314	3201594.34	37.64	325	1620	38
1315	3211599.29	37.94	326	1625	38
1316	3221604.43	37.93	327	1630	38
1317	3231609.42	38.05	328	1635	38
			329	1640	38
			330	1645	38
			331	1650	38
			332	1655	38
			333	1660	38
			334	1665	38
			335	1670	38
			336	1675	38
			337	1680	38
			338	1685	38

Appendix C cont.

339	1690	38
340	1695	38
341	1700	38
342	1705	38
343	1710	38
344	1715	38
345	1720	38
346	1725	38
347	1730	38
348	1735	38
349	1740	38
350	1745	38
351	1750	38
352	1755	38
353	1760	38
354	1765	38
355	1770	38
356	1775	38
357	1780	38
358	1785	38
359	1790	38
360	1795	38
361	1800	38
362	1805	38
363	1810	38
364	1815	38
365	1820	38
366	1825	38
367	1830	38
368	1835	38
369	1840	38
370	1845	38
371	1850	38
372	1855	38
373	1860	38
374	1865	38
375	1870	38
376	1875	38
377	1880	38
378	1885	38
379	1890	38
380	1895	38
381	1900	38
382	1905	38
383	1910	38
384	1915	38
385	1920	38
386	1925	38
387	1930	38
388	1935	38
389	1940	38
390	1945	38
391	1950	38
392	1955	38
393	1960	38
394	1965	38

Appendix C cont.

395	1970	38
396	1975	38
397	1980	38
398	1985	38
399	1990	38
400	1995	38
401	2000	38
402	2005	38
403	2010	38
404	2015	38
405	2020	38
406	2025	38
407	2030	38
408	2035	38
409	2040	38
410	2045	38
411	2050	38
412	2055	38
413	2060	38

Note: FFID is the field file identification number. Distance and elevation are in meters. SP refers to shot point. Geo refers to geophone.

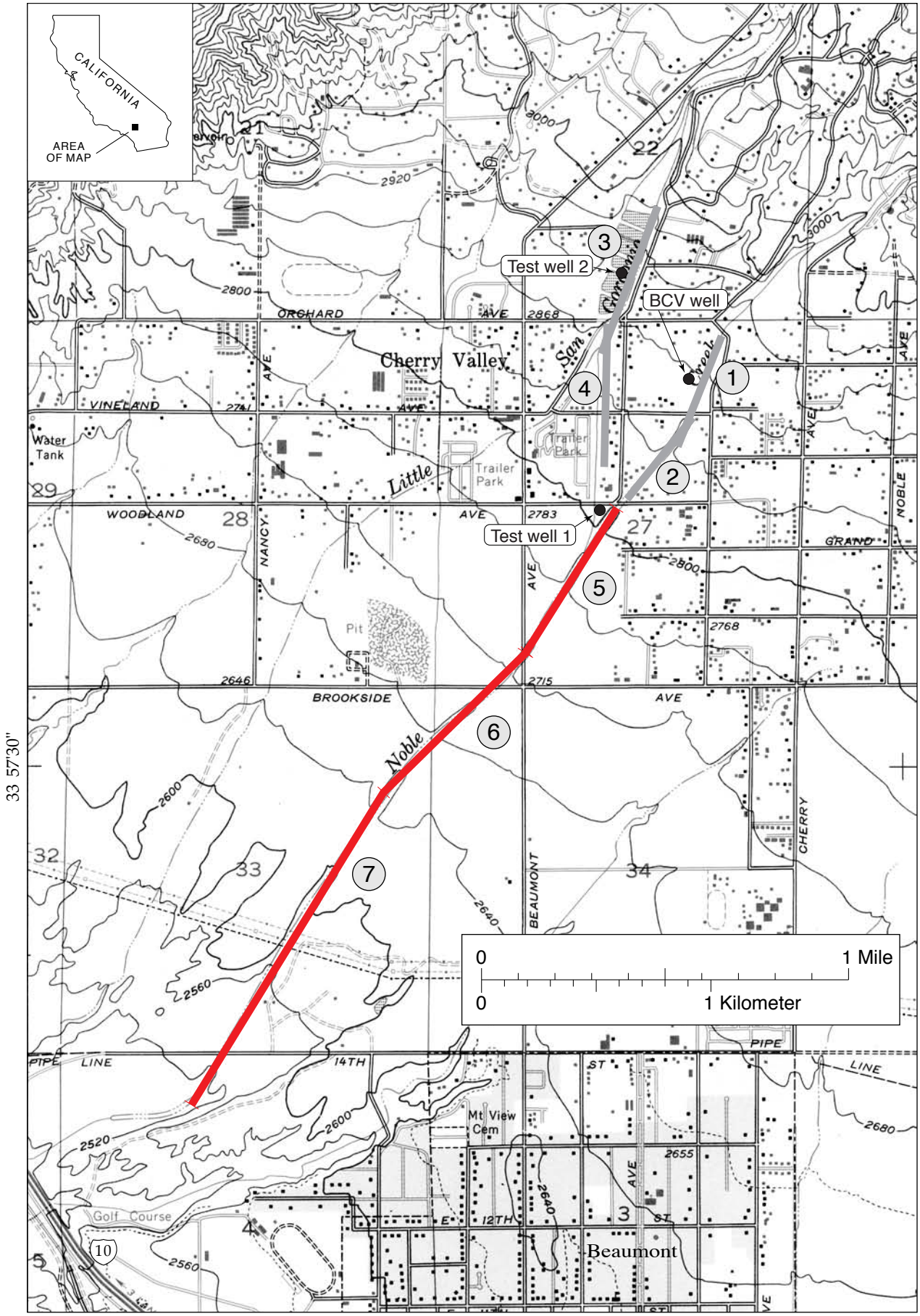
117 00'
116 57'30"
33 57'30"
CALIFORNIA
AREA OF MAP
Test well 2
BCV well
Test well 1
Cherry Valley
Little
Noble
Trailer Park
Water Tank
Pit
Mt View Cem
Golf Course
Beaumont
ORCHARD
VINELAND
WOODLAND
BROOKSIDE
NANCY
BEAUMONT
CHERRY
NOBLE
GRAND
14TH
12TH
PIPE LINE
1
2
3
4
5
6
7
0
1 Mile
0
1 Kilometer

Figure 1a

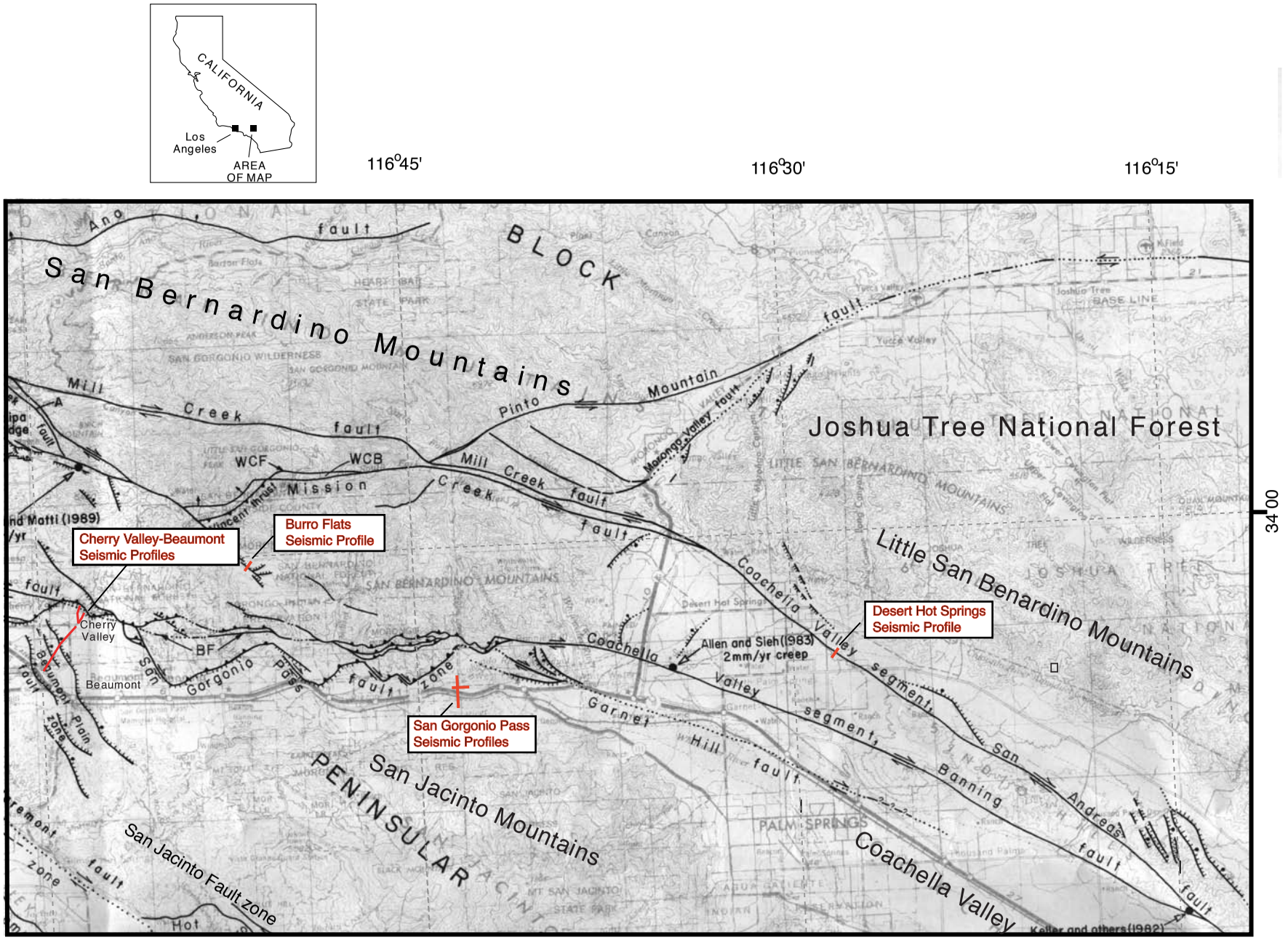
CALIFORNIA
Los Angeles
AREA OF MAP
116°45'
116°30'
116°15'
34°00
San Bernardino Mountains
BLOCK
Joshua Tree National Forest
Little San Benardino Mountains
San Jacinto Mountains
PENINSULAR RANGES
Coachella Valley
San Jacinto Fault Zone
Cherry Valley-Beaumont Seismic Profiles
Burro Flats Seismic Profile
San Gorgonio Pass Seismic Profiles
Desert Hot Springs Seismic Profile
Allen and Sieh (1983) 2mm/yr creep
Keller and others (1982)
Mill Creek fault
Mission Creek fault
Pinto Mountain fault
Morongo Valley fault
Banning fault
San Andreas fault
Garnet Hill fault
Coachella Valley segment
WCF
WCB
BF
Cherry Valley
Beaumont
PALM SPRINGS

Figure 1b

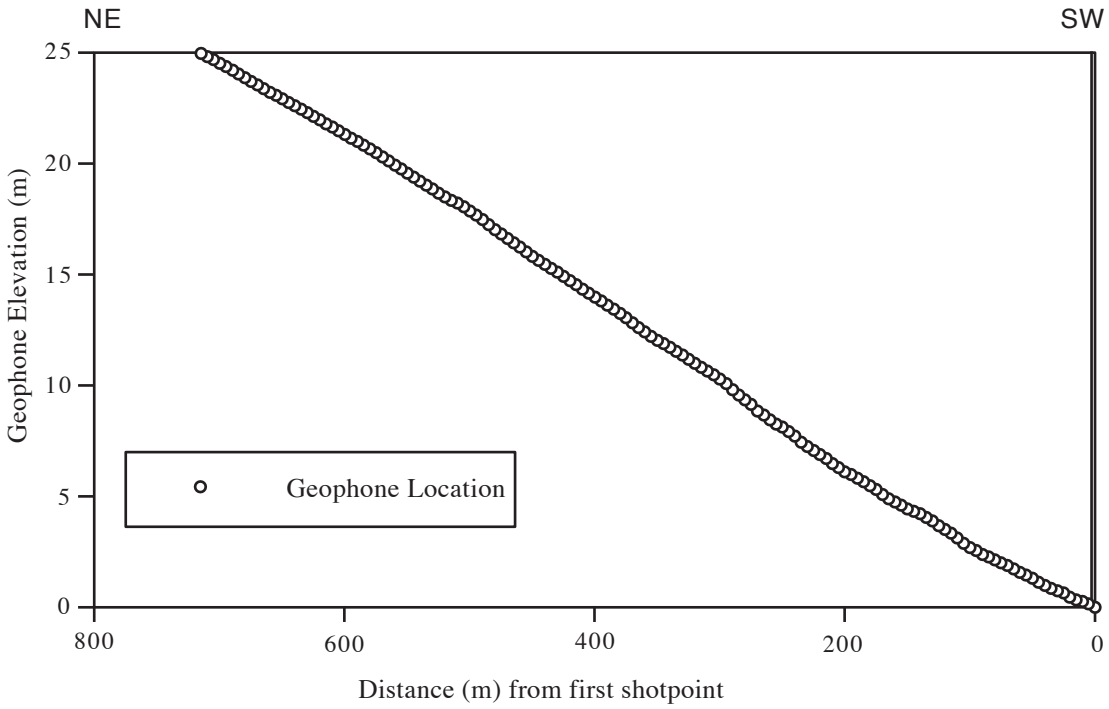

Figure 2

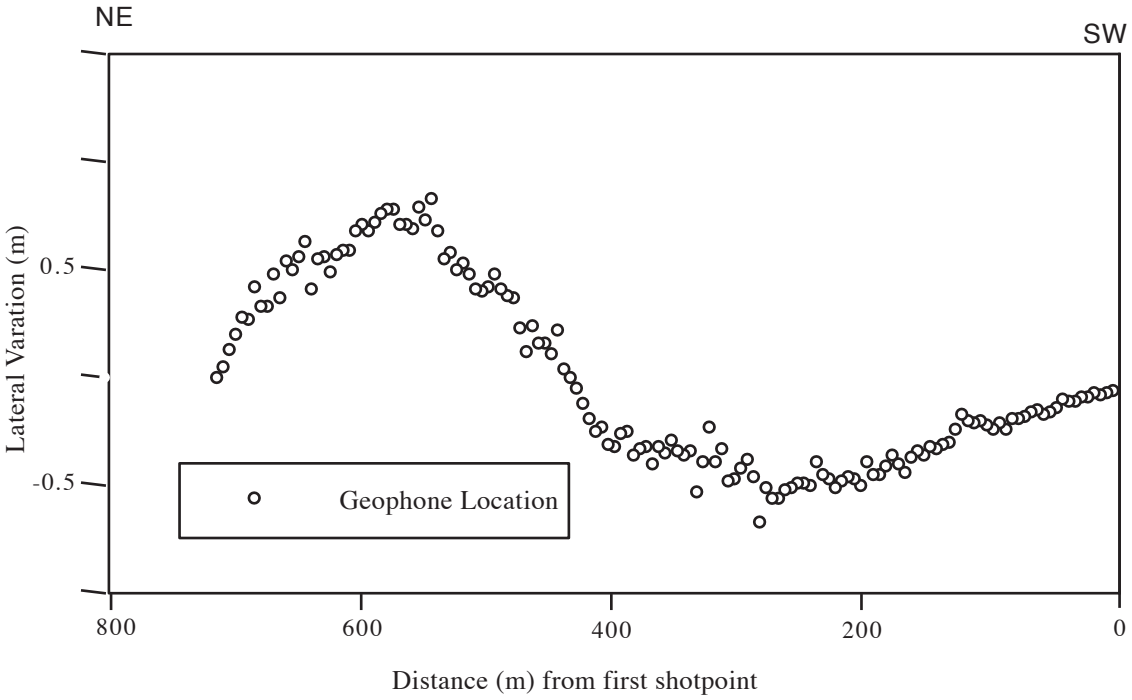

Figure.3

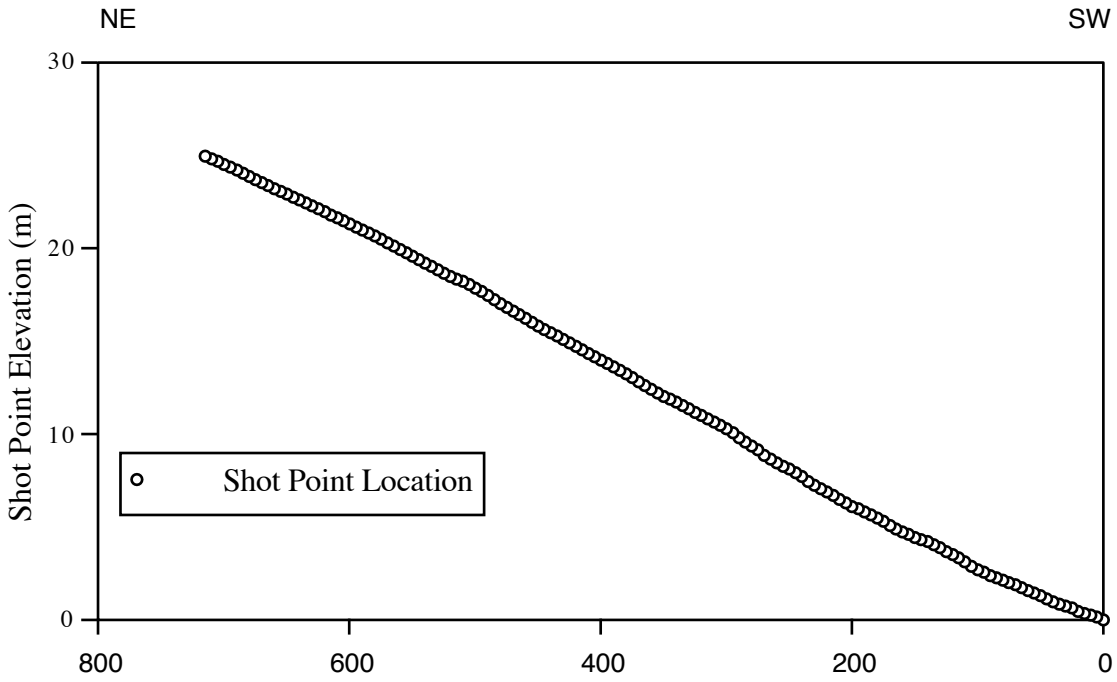

Figure. 4

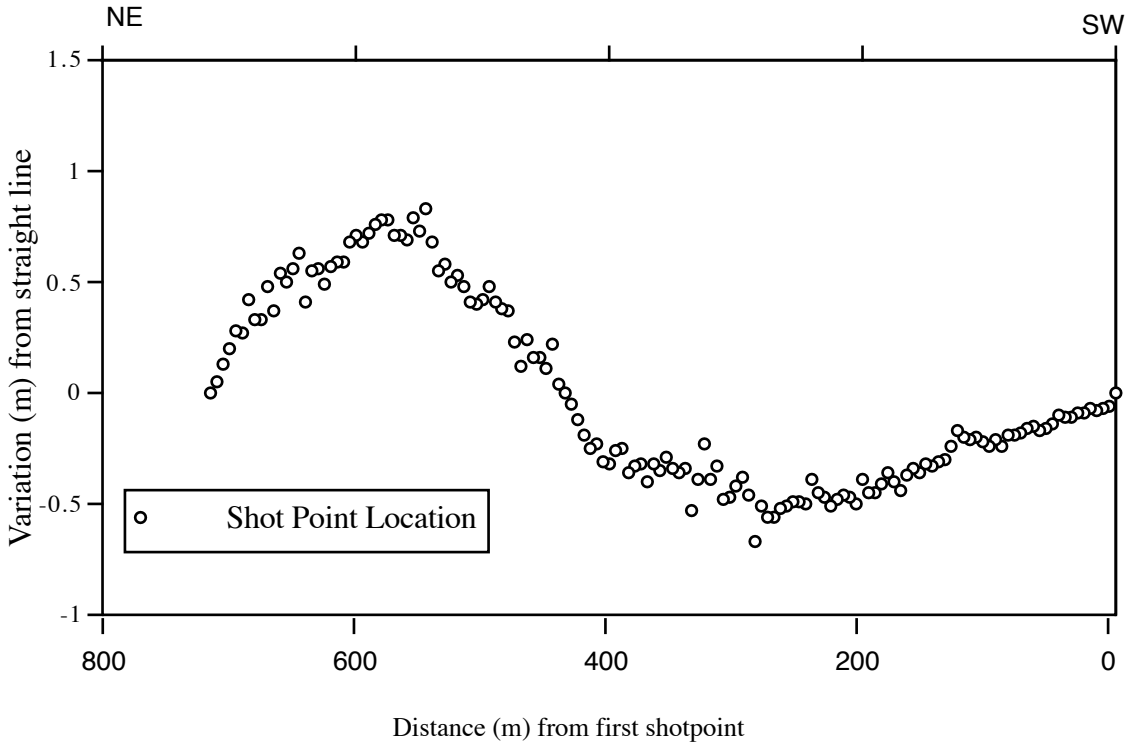

Figure. 5

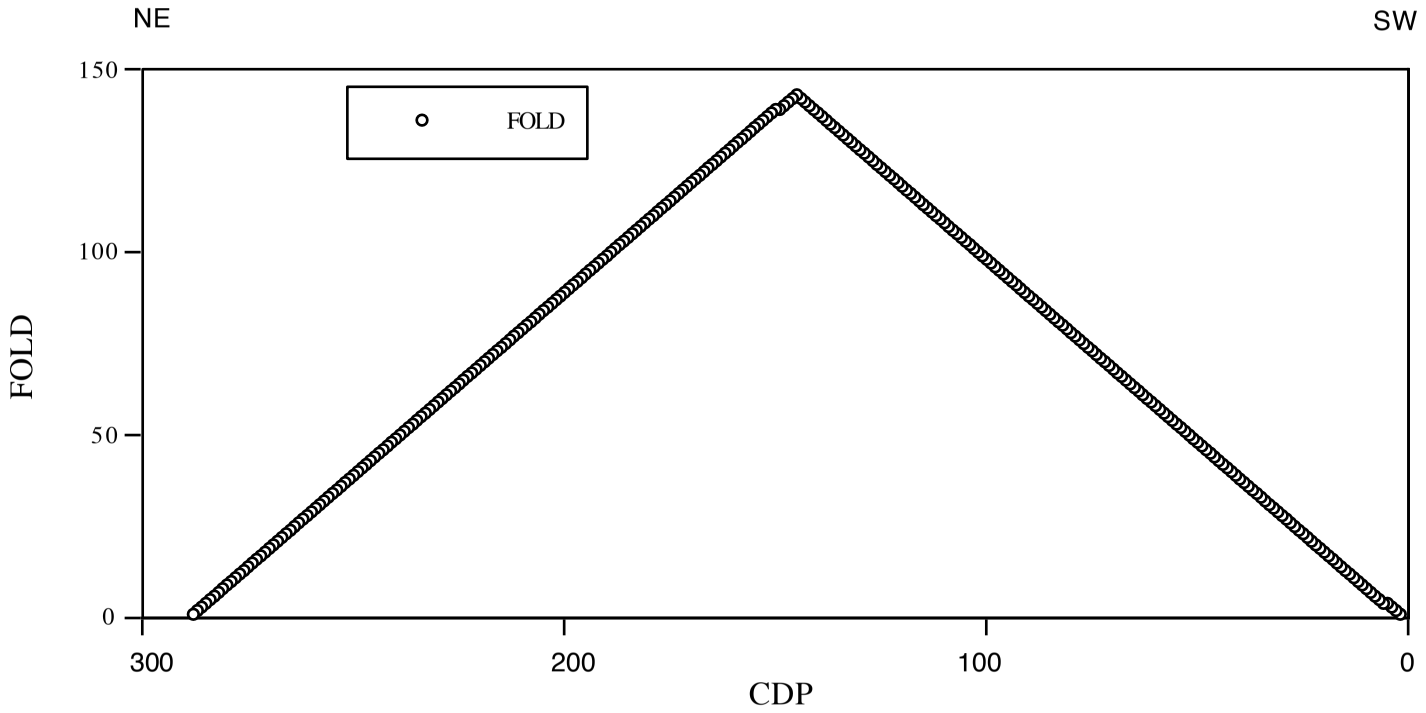

Figure 6

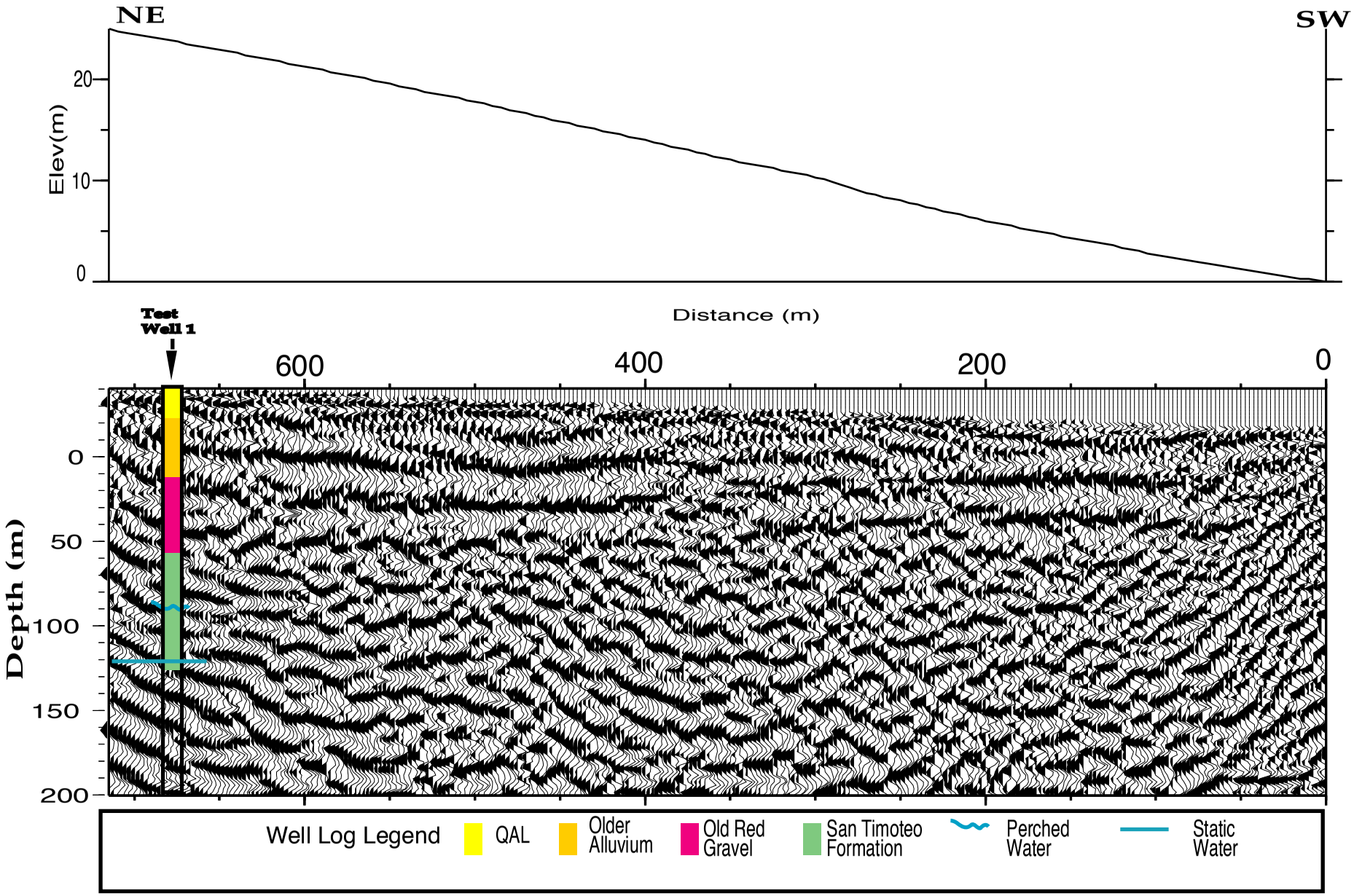
NE
SW
Elev(m)
20
10
0
Test Well 1
Distance (m)
600
400
200
0
Depth (m)
0
50
100
150
200
Well Log Legend
QAL
Older Alluvium
Old Red Gravel
San Timoteo Formation
Perched Water
Static Water

Figure. 7

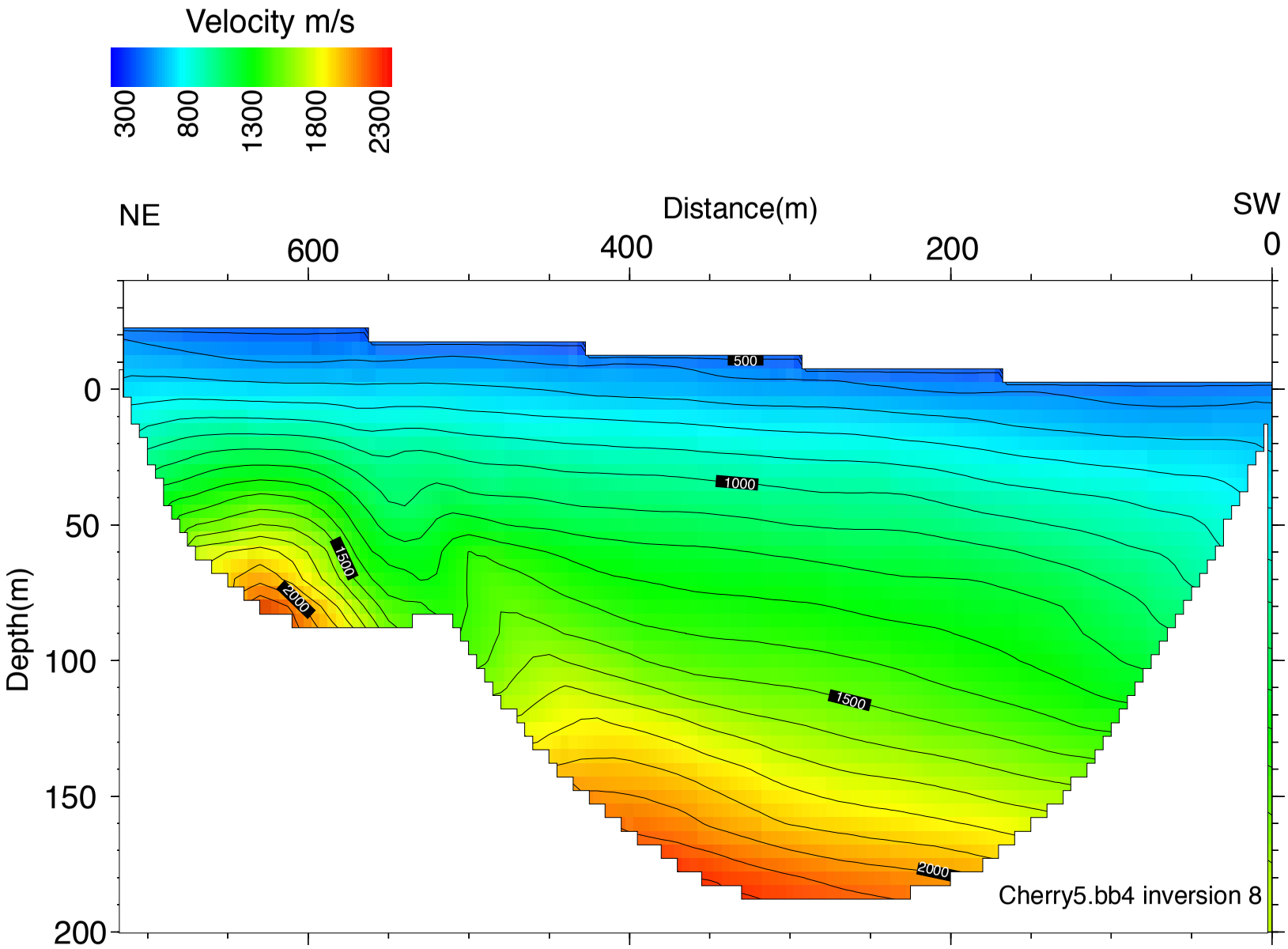
Velocity m/s
300
800
1300
1800
2300
NE
Distance(m)
SW
600
400
200
0
Depth(m)
0
50
100
150
200
500
1000
1500
2000
1500
2000
Cherry5.bb4 inversion 8

Figure 8

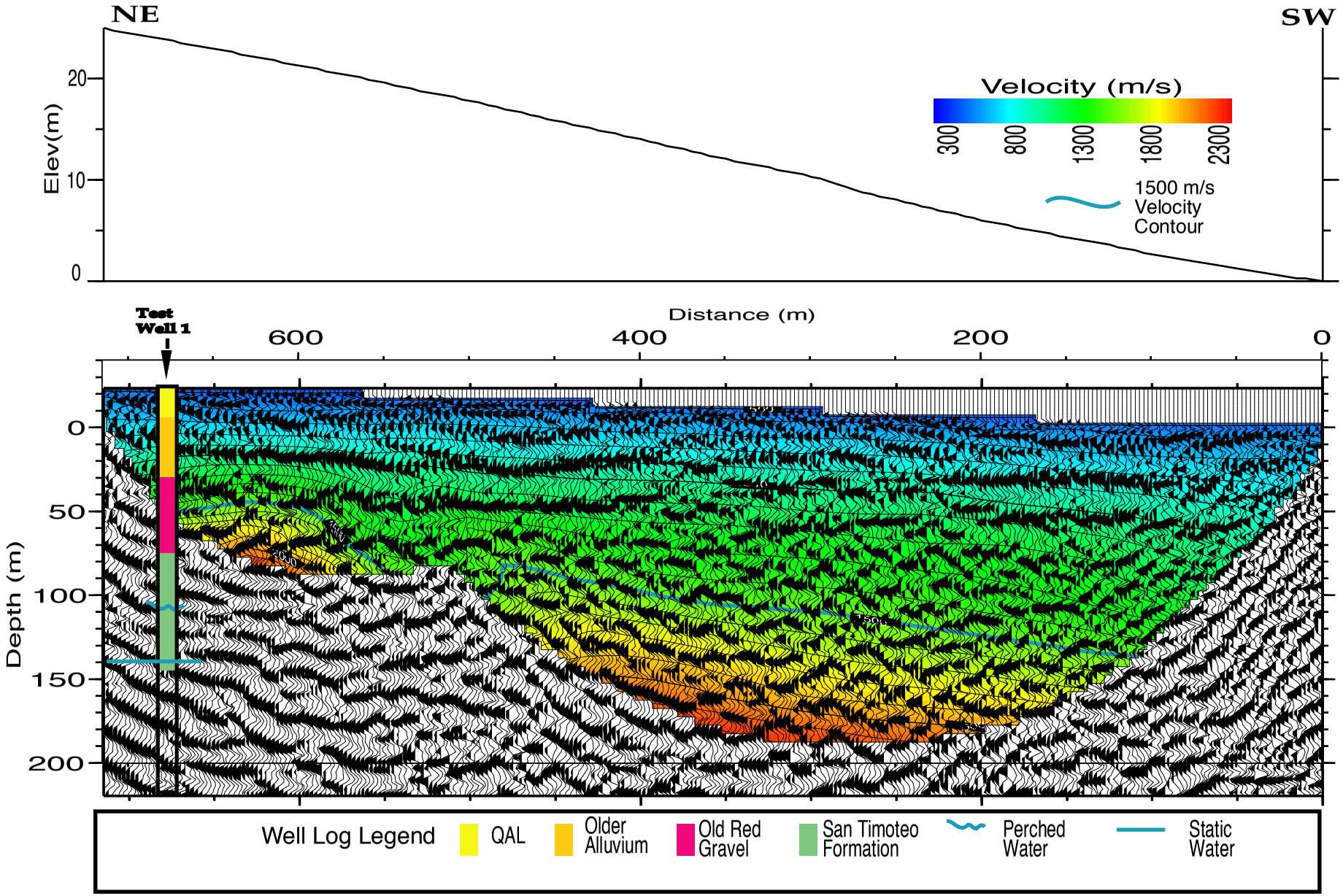
NE
SW
Elev(m)
20
10
0
Velocity (m/s)
300
800
1300
1800
2300
1500 m/s
Velocity
Contour
Test
Well 1
Distance (m)
600
400
200
0
Depth (m)
0
50
100
150
200
Well Log Legend
QAL
Older
Alluvium
Old Red
Gravel
San Timoteo
Formation
Perched
Water
Static
Water

Figure. 9

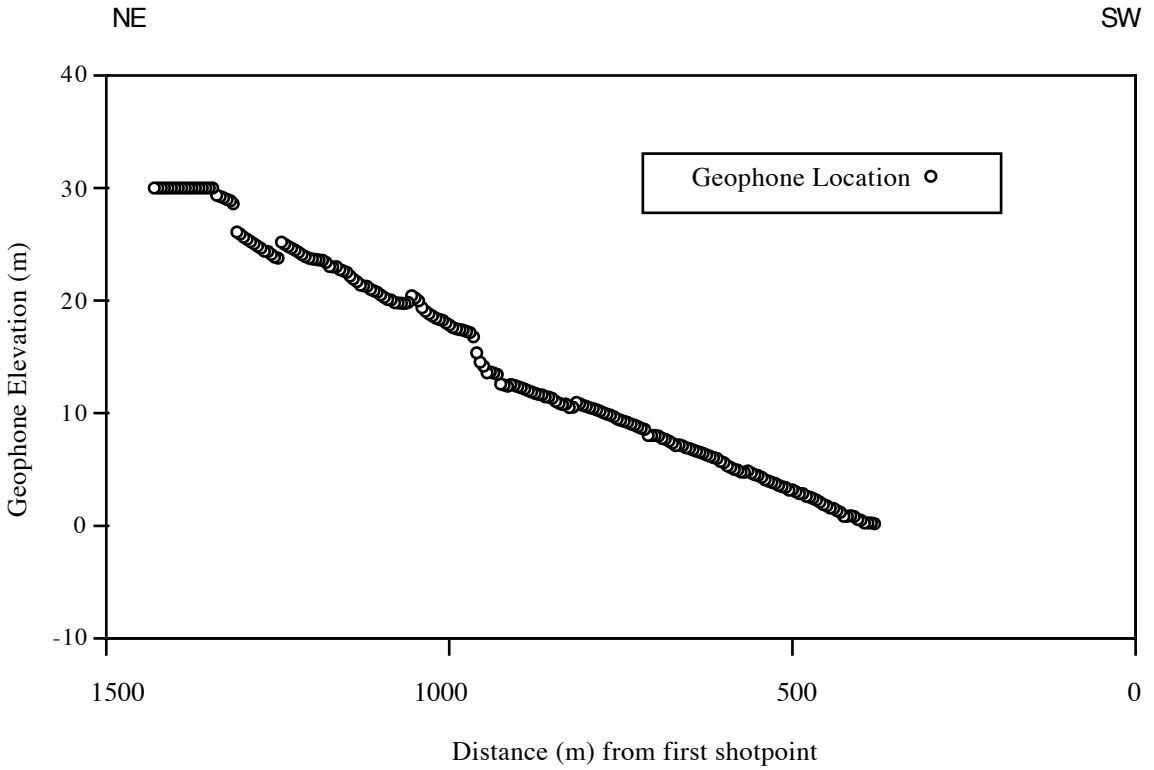

Figure 10

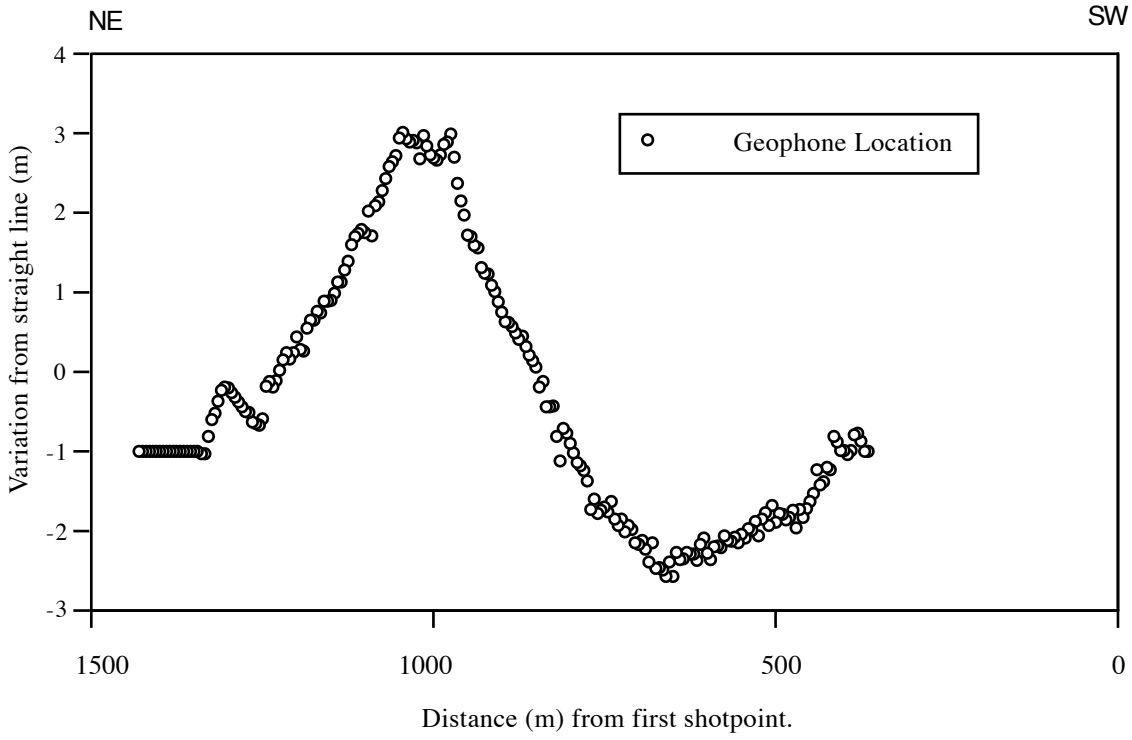

Figure 11

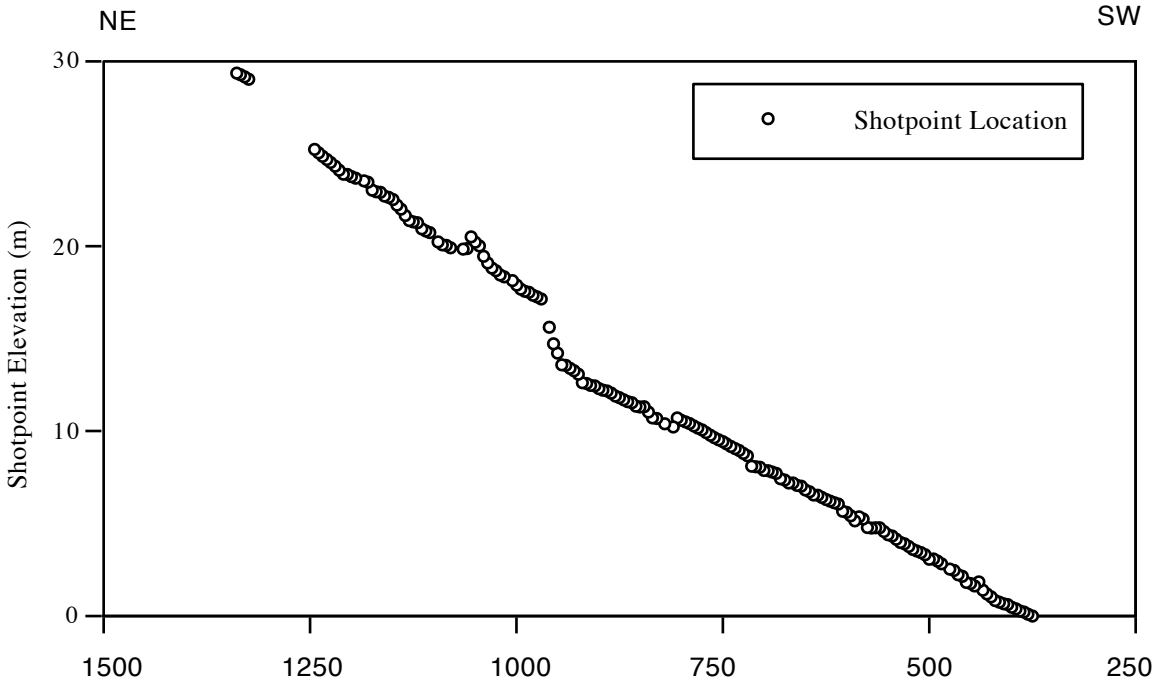

Figure 12

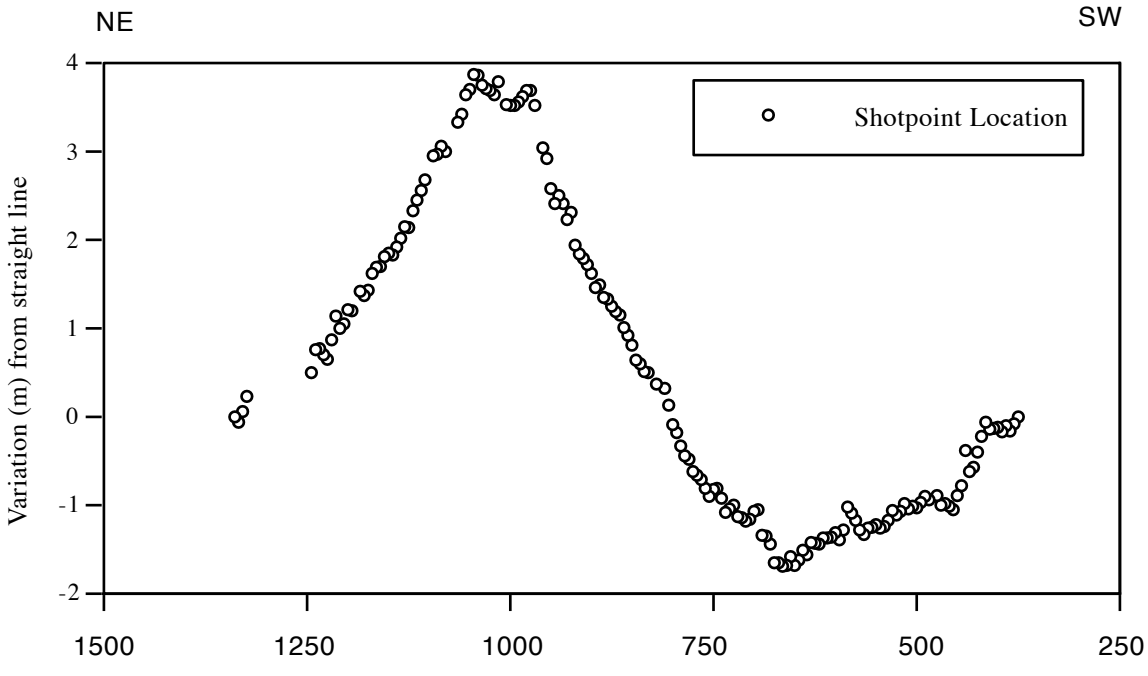

Figure 13

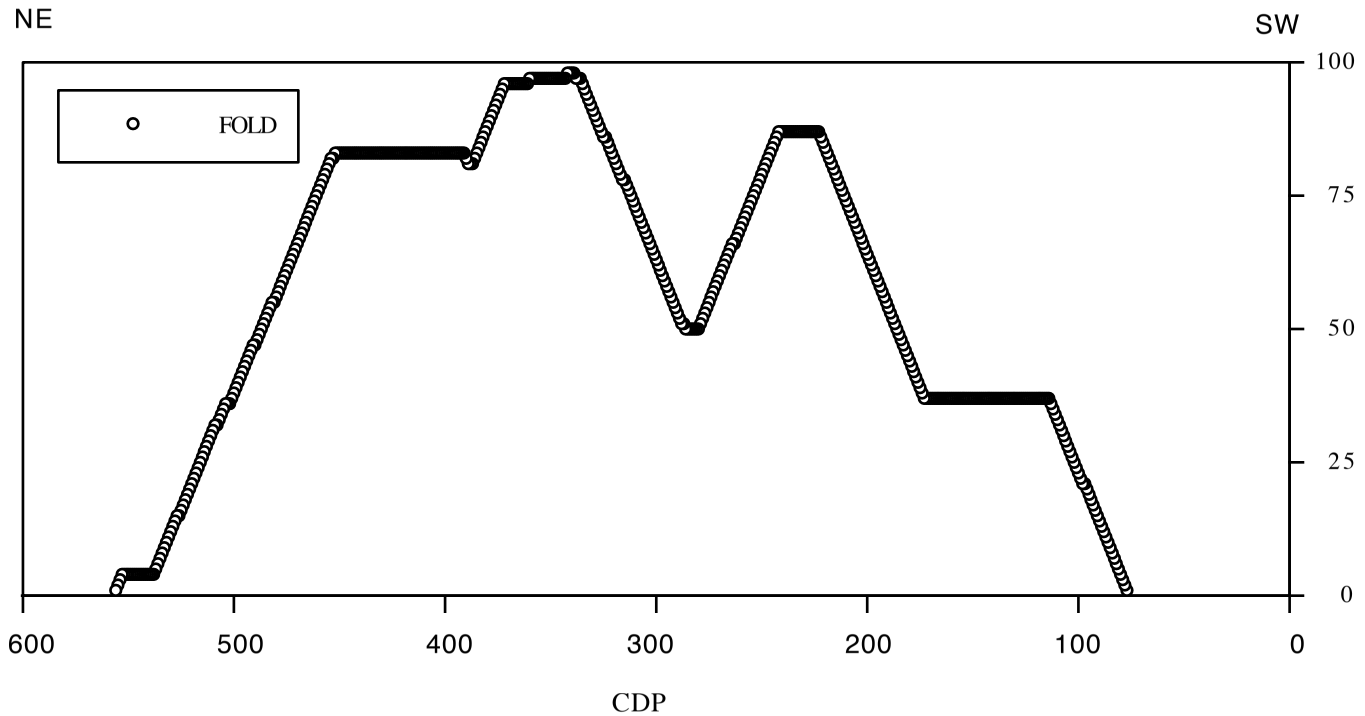

Figure 14

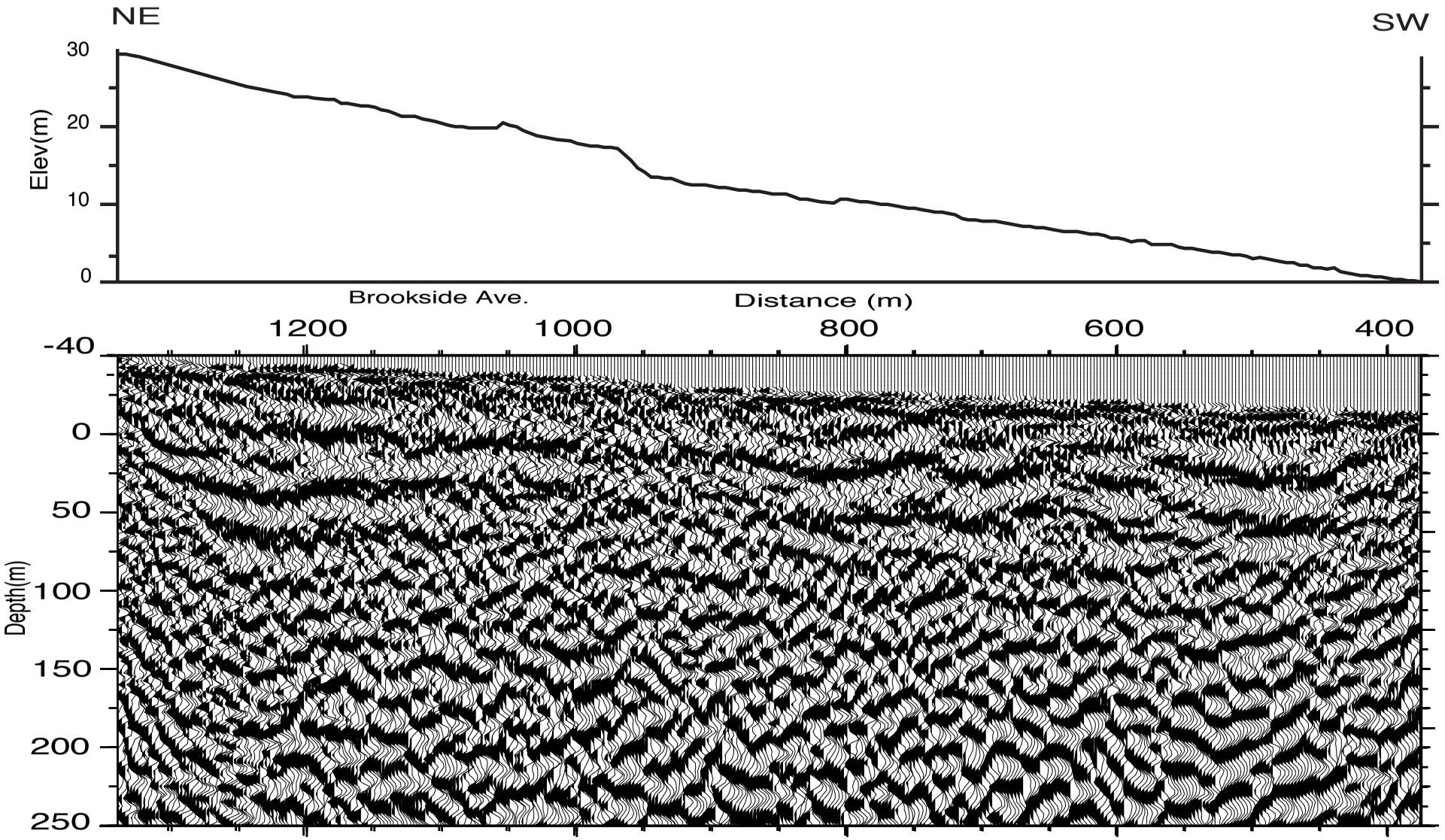
NE
SW
30
20
10
0
Elev(m)
Brookside Ave.
Distance (m)
1200
1000
800
600
400
-40
0
50
100
150
200
250
Depth(m)

Figure 15

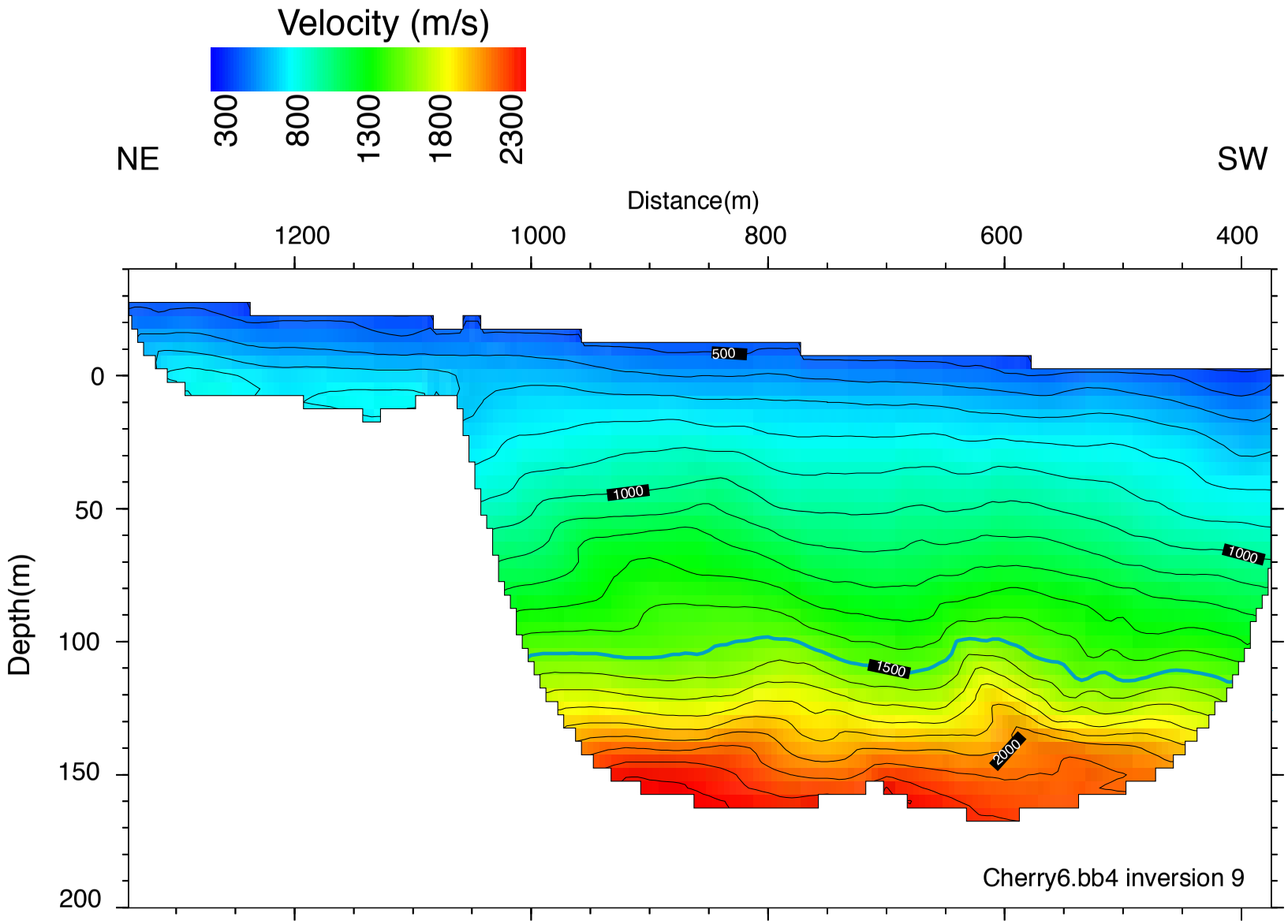
Velocity (m/s)
300
800
1300
1800
2300
NE
SW
Distance(m)
1200
1000
800
600
400
0
50
100
150
200
Depth(m)
500
1000
1000
1500
2000
Cherry6.bb4 inversion 9

Figure 16

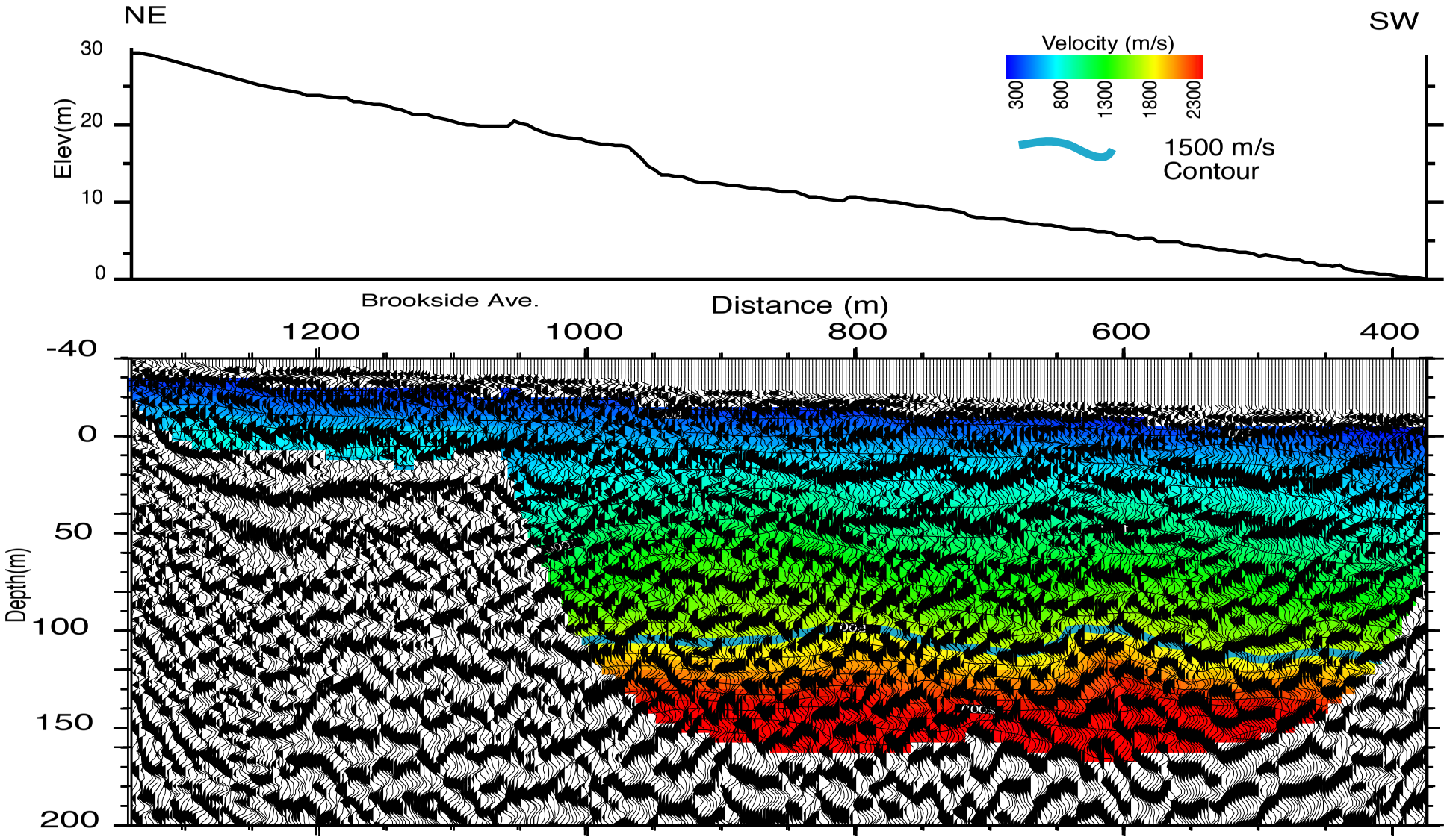
NE
SW
Velocity (m/s)
300
800
1300
1800
2300
1500 m/s
Contour
Elev(m)
30
20
10
0
Brookside Ave.
Distance (m)
1200
1000
800
600
400
-40
0
50
100
150
200
Depth(m)

Figure 17

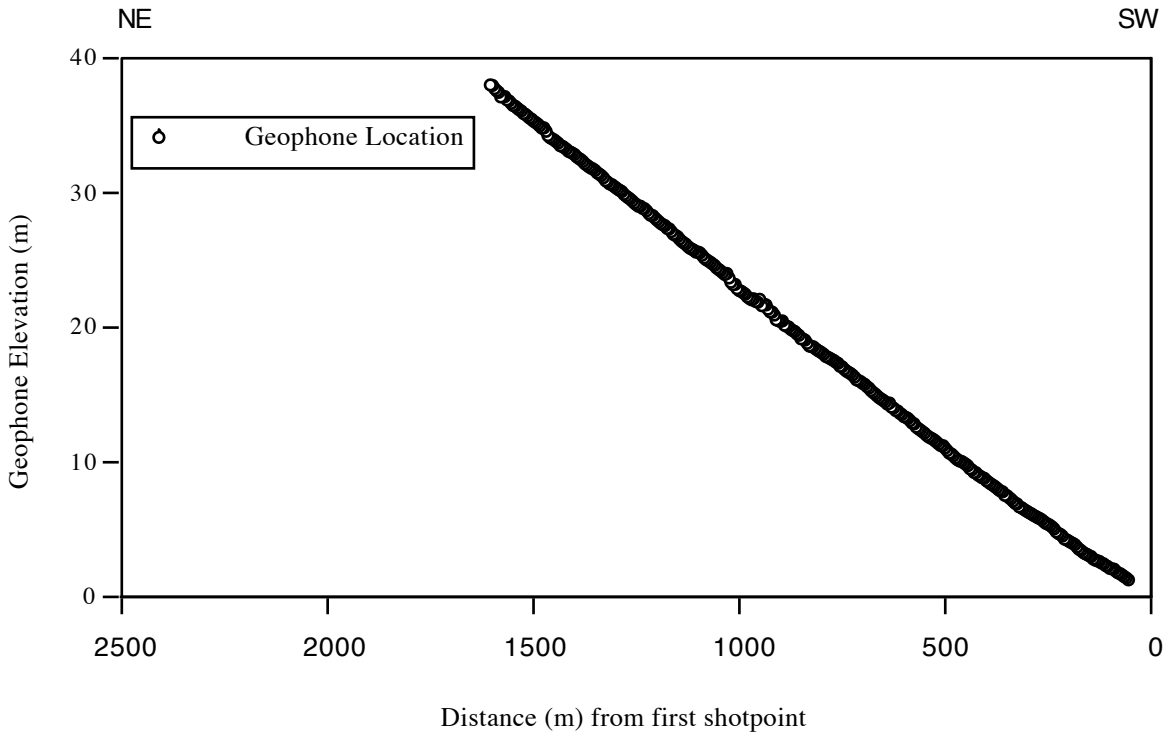

Figure 18

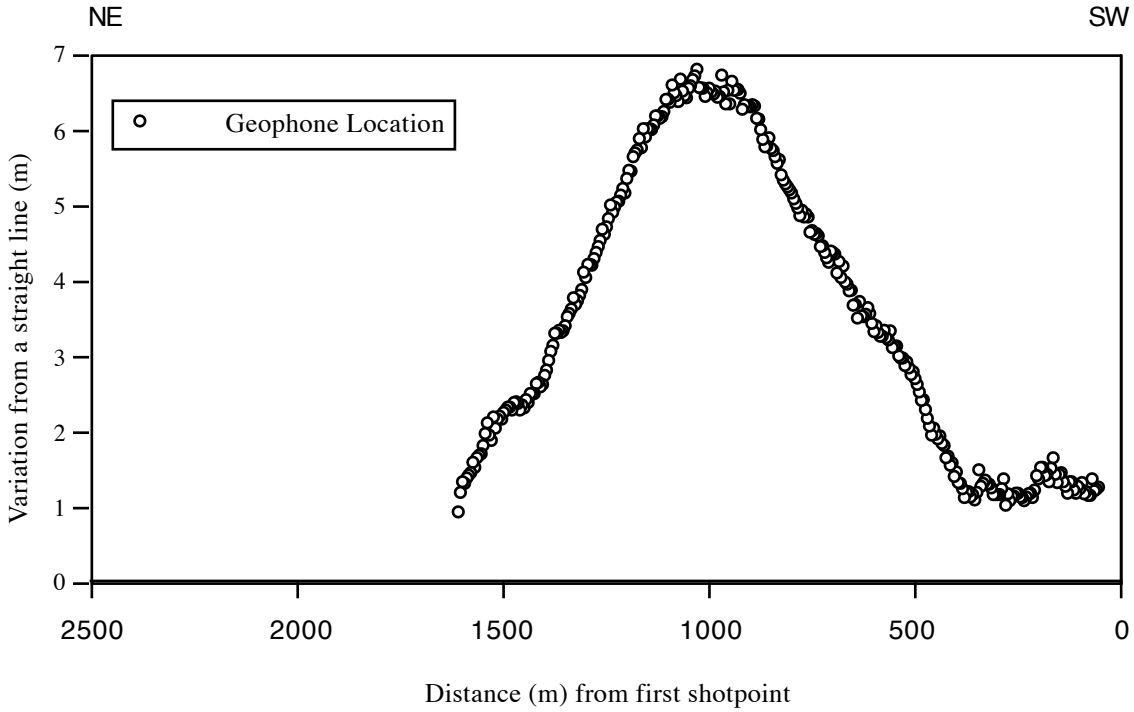

Figure 19

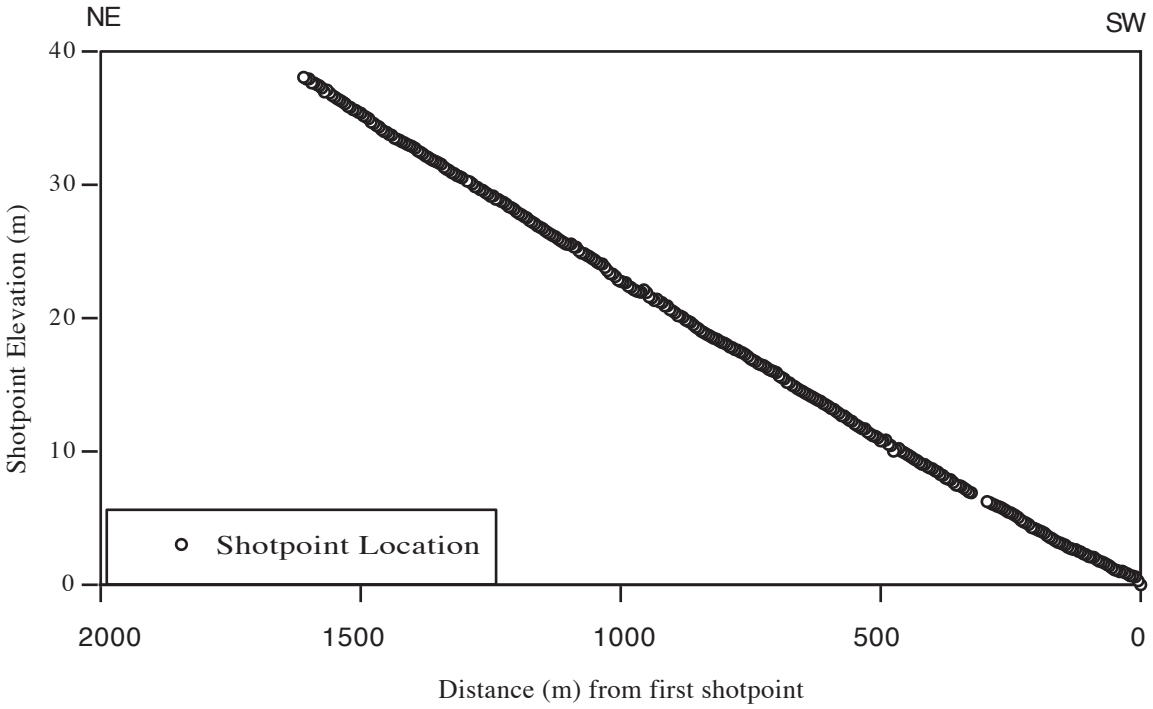

Figure 20

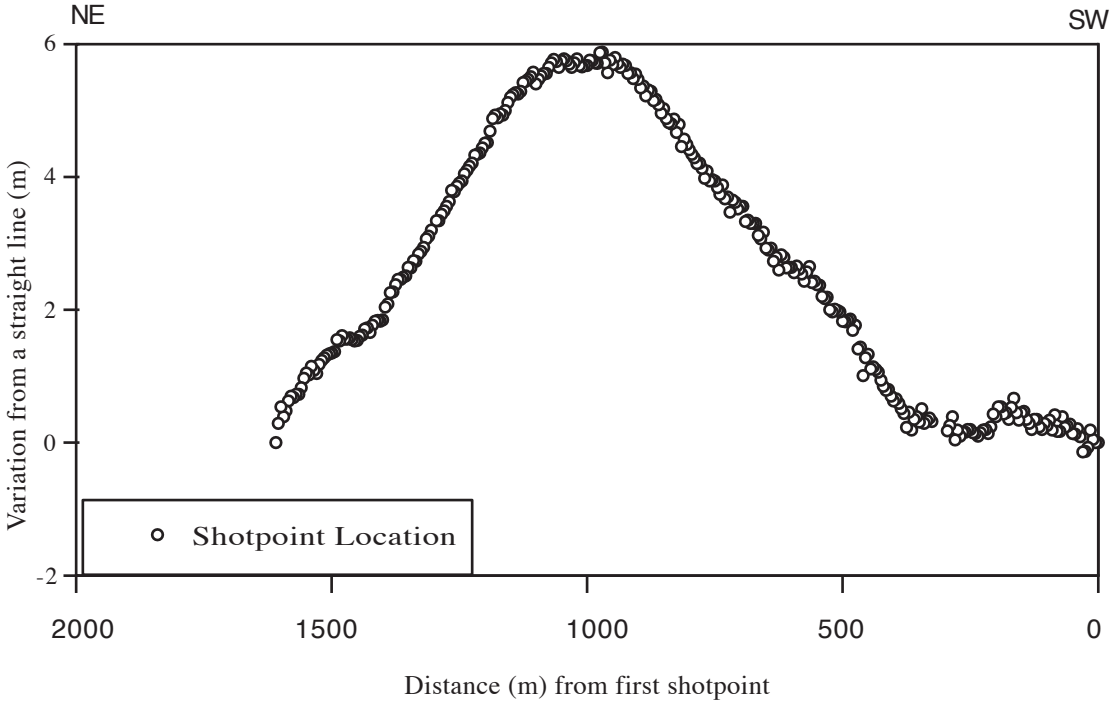

Figure 21

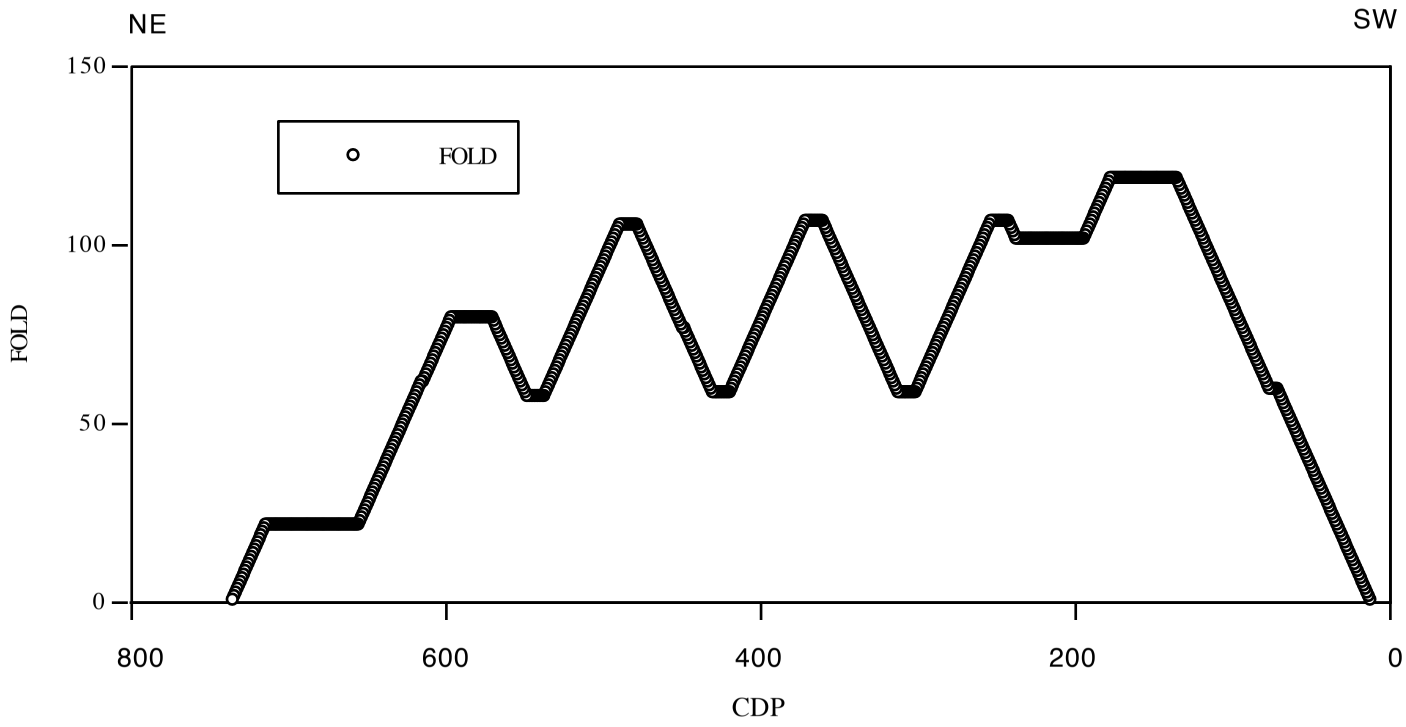

Figure 22

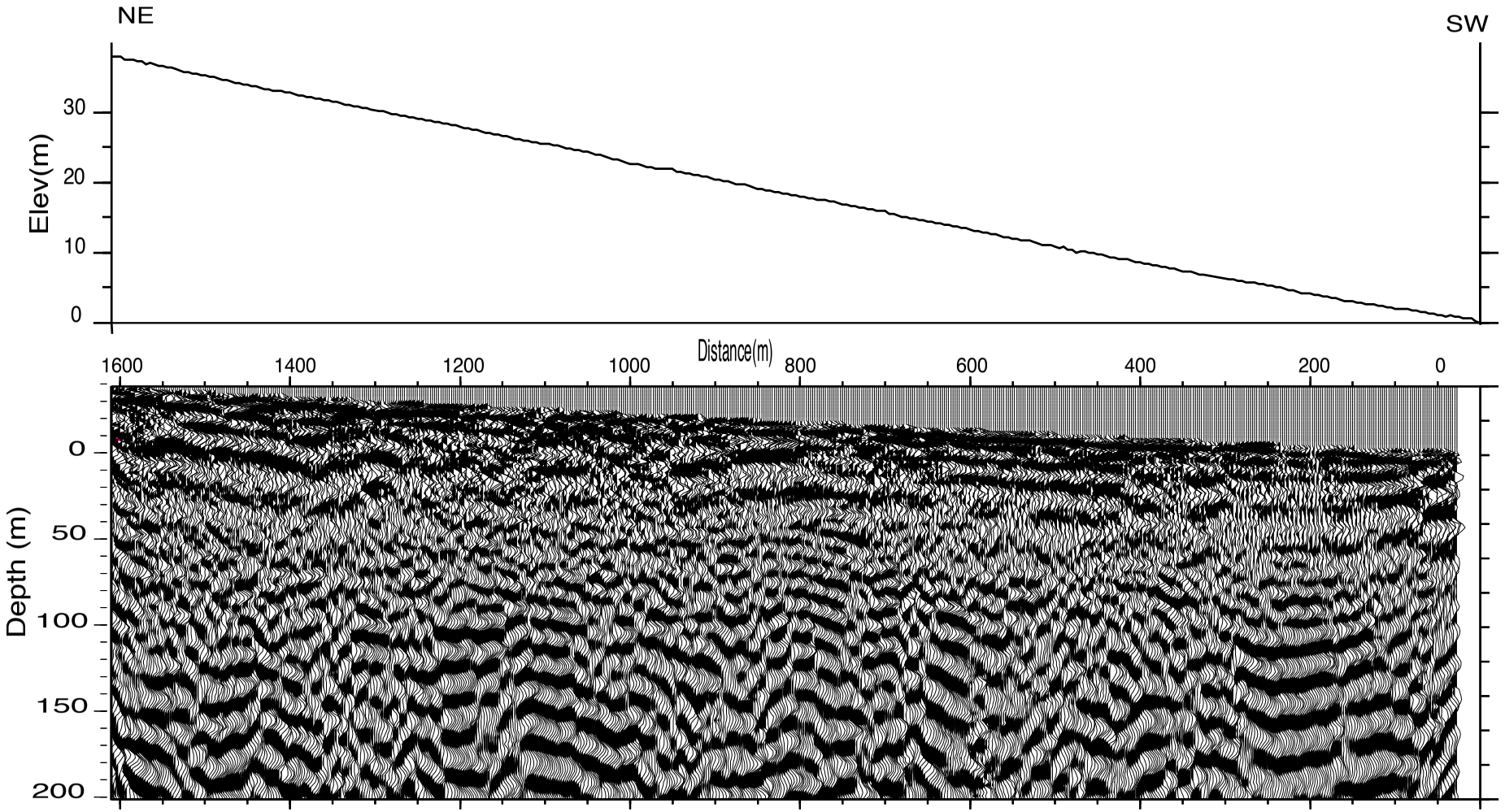
NE
SW
Elev(m)
30
20
10
0
Distance(m)
1600
1400
1200
1000
800
600
400
200
0
Depth (m)
0
50
100
150
200

Figure 23

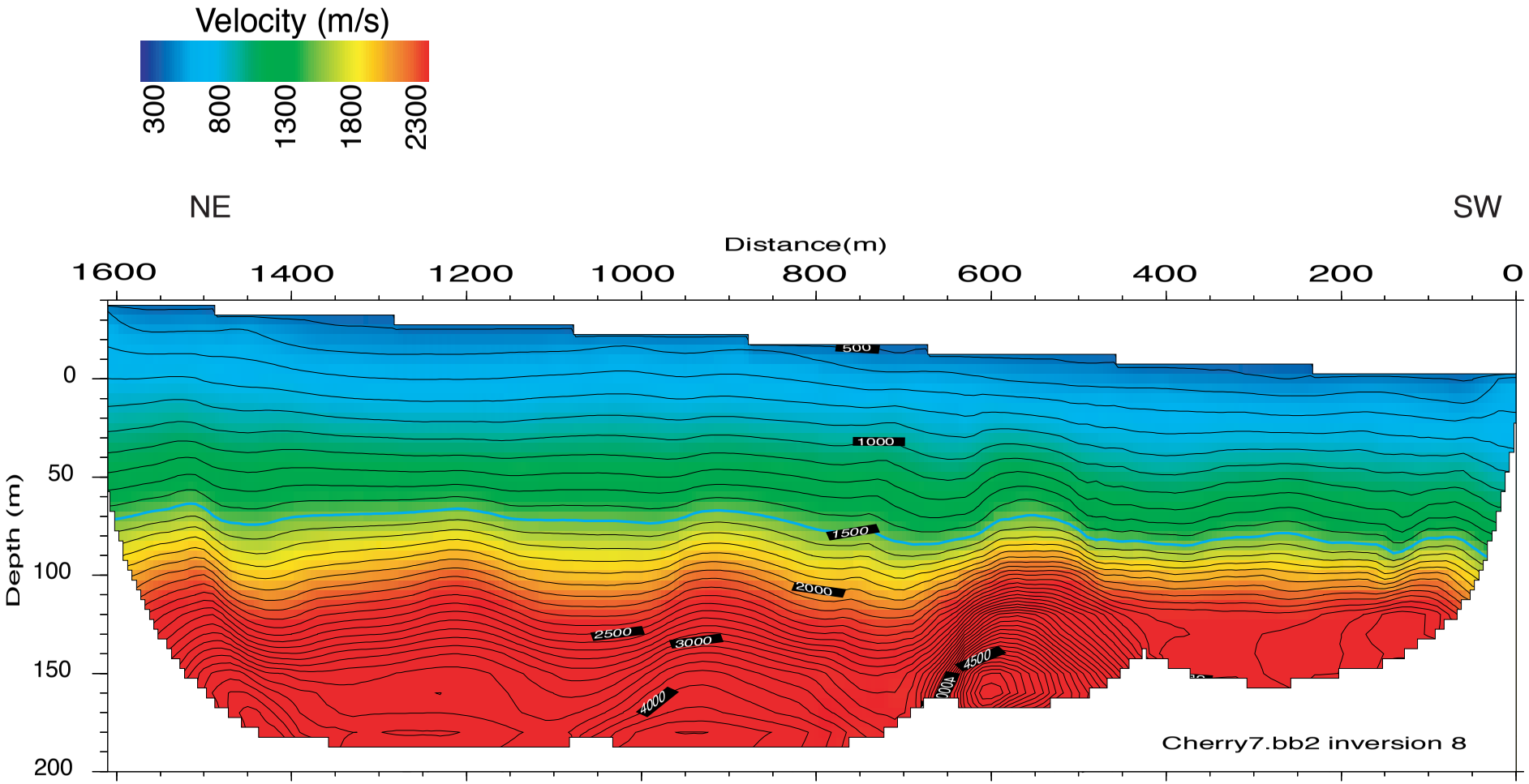
Velocity (m/s)
300
800
1300
1800
2300
NE
SW
Distance(m)
1600
1400
1200
1000
800
600
400
200
0
Depth (m)
0
50
100
150
200
500
1000
1500
2000
2500
3000
4000
4500
Cherry7.bb2 inversion 8

Figure 24

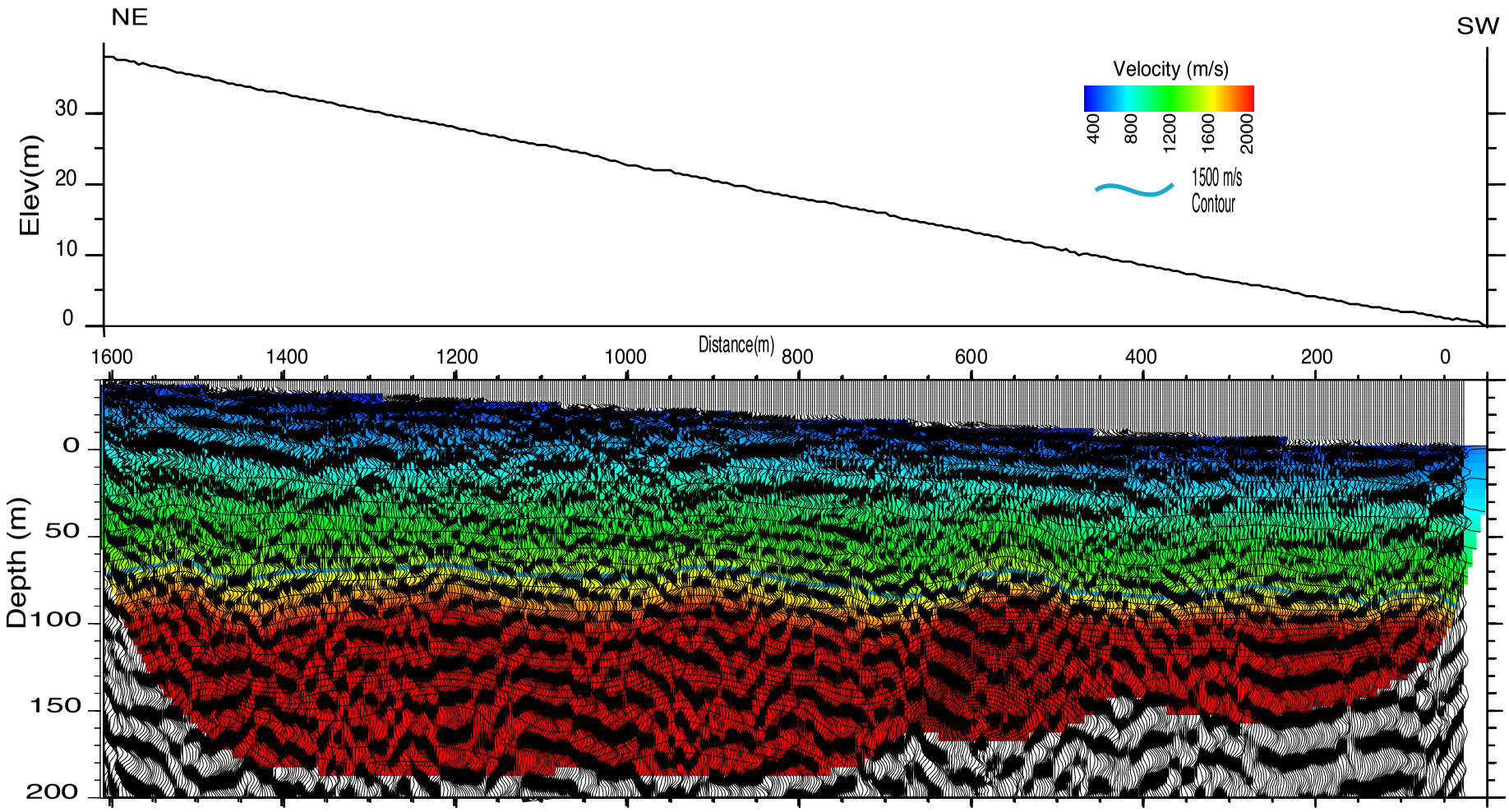
NE
SW
Velocity (m/s)
400
800
1200
1600
2000
1500 m/s
Contour
Elev(m)
30
20
10
0
Distance(m)
1600
1400
1200
1000
800
600
400
200
0
Depth (m)
0
50
100
150
200

Figure 25

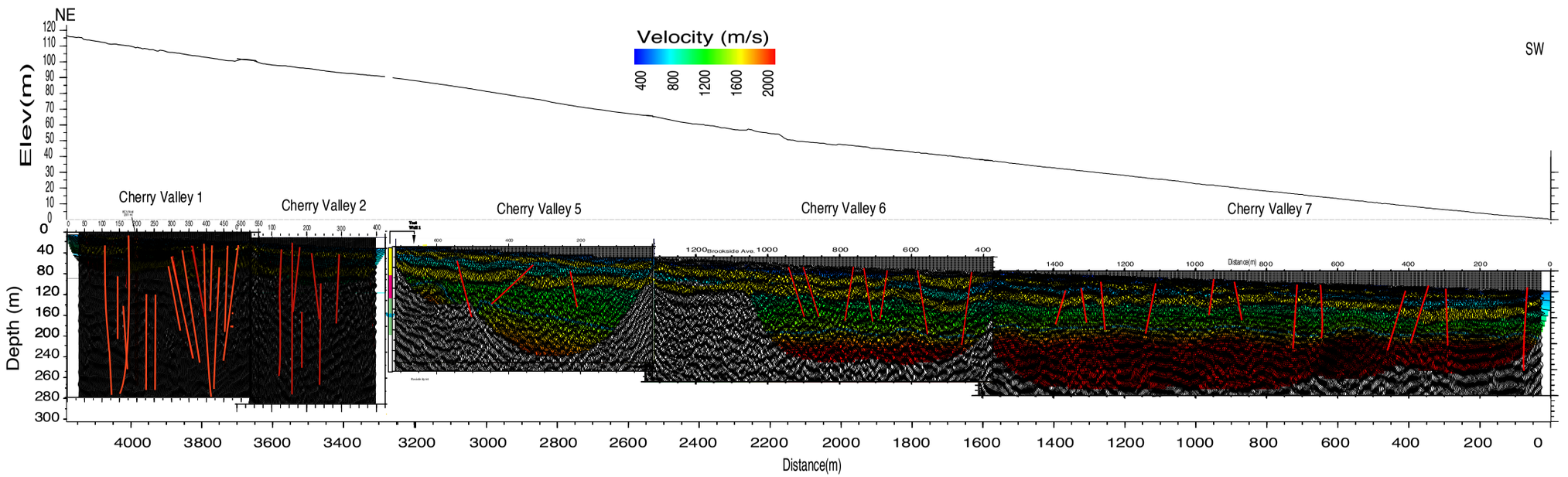
NE
SW
Velocity (m/s)
400
800
1200
1600
2000
Elev(m)
Cherry Valley 1
Cherry Valley 2
Cherry Valley 5
Cherry Valley 6
Cherry Valley 7
Brookside Ave.
Depth (m)
Distance(m)

Figure 26a

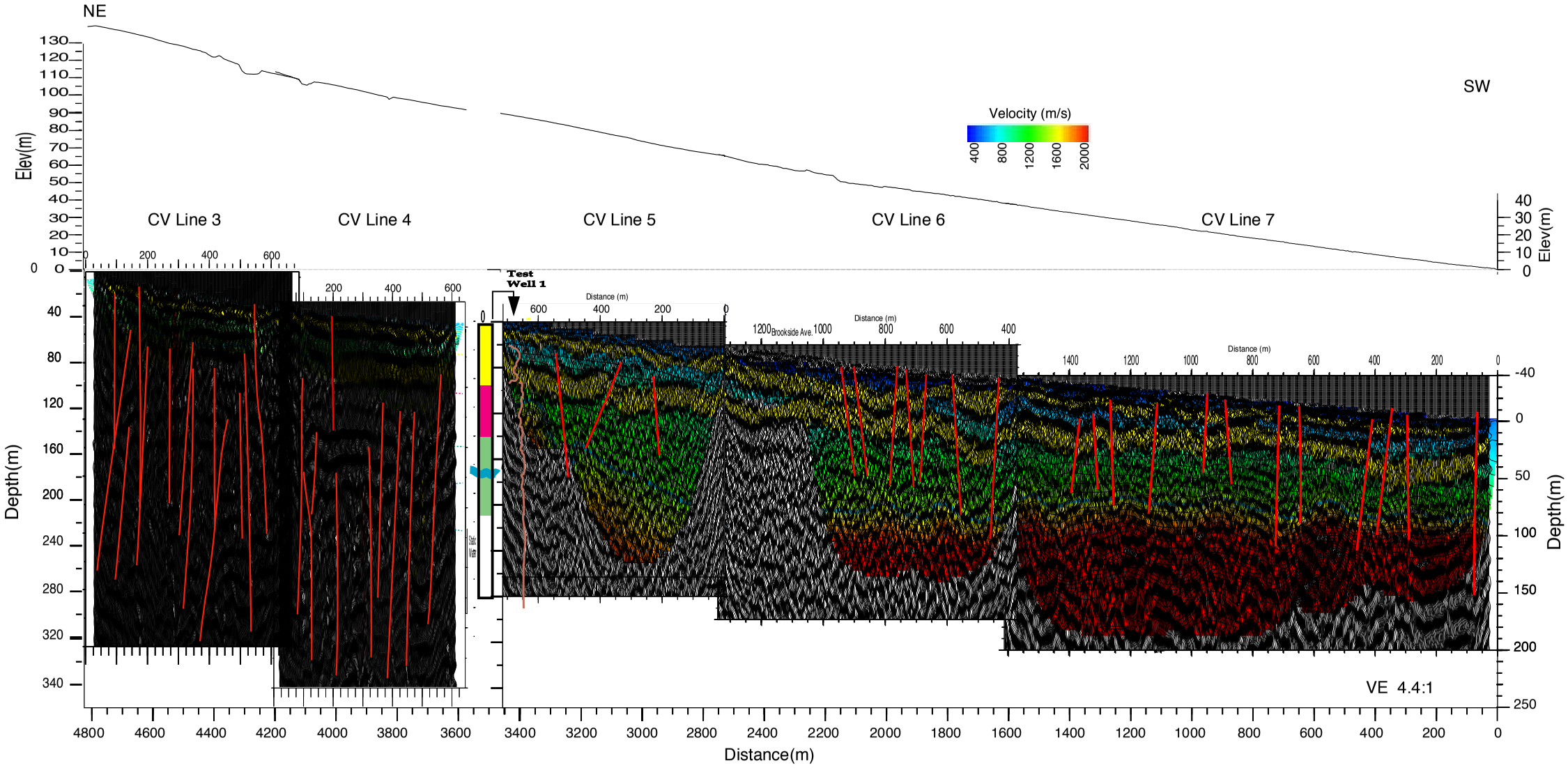
NE
SW
Elev(m)
CV Line 3
CV Line 4
CV Line 5
CV Line 6
CV Line 7
Velocity (m/s)
400
800
1200
1600
2000
Test Well 1
Distance (m)
Brookside Ave.
Depth(m)
VE 4.4:1
Distance(m)

Figure 26b

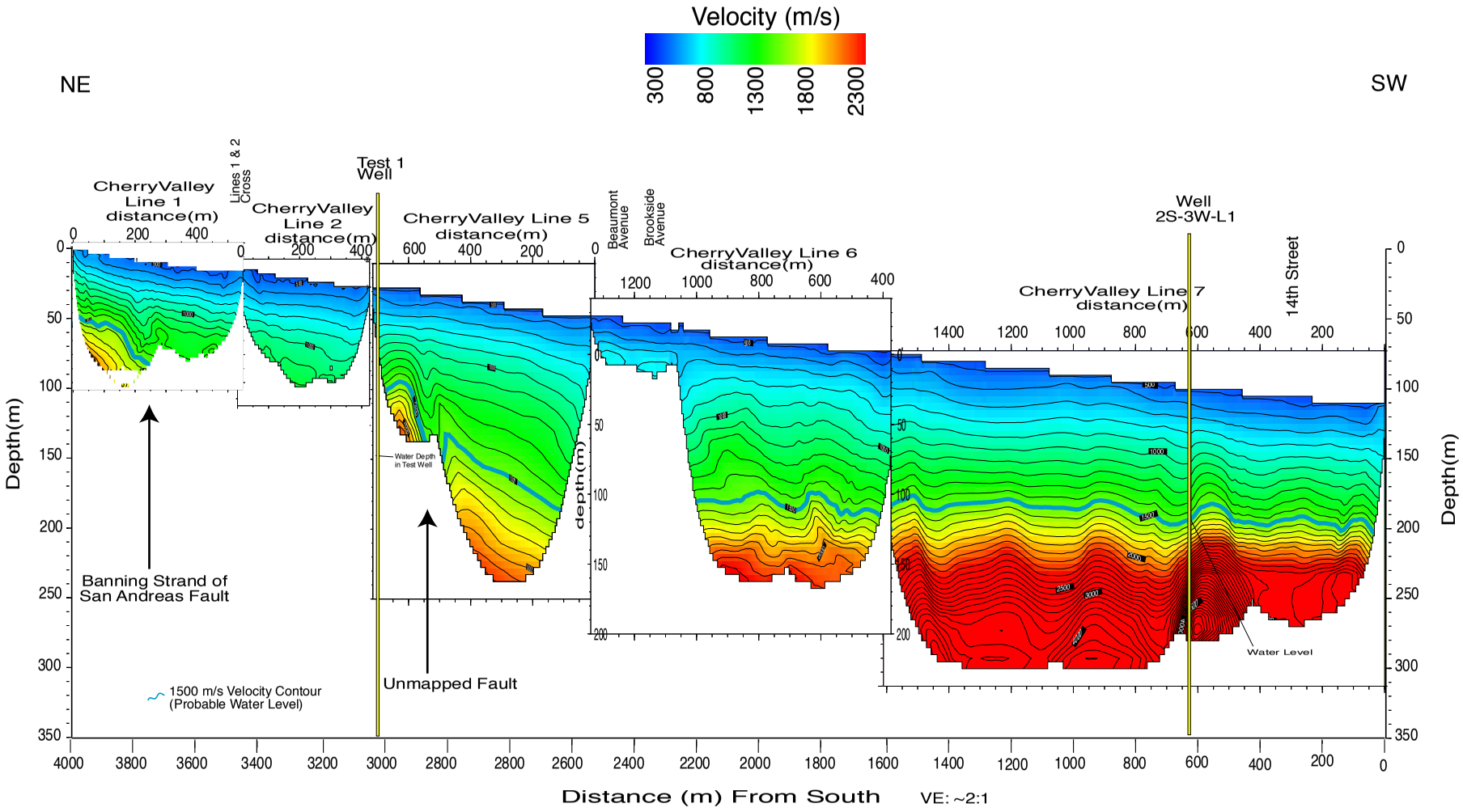
Velocity (m/s)
300
800
1300
1800
2300
NE
SW
CherryValley Line 1 distance(m)
Lines 1 & 2 Cross
CherryValley Line 2 distance(m)
Test 1 Well
CherryValley Line 5 distance(m)
Beaumont Avenue
Brookside Avenue
CherryValley Line 6 distance(m)
Well 2S-3W-L1
CherryValley Line 7 distance(m)
14th Street
Depth(m)
Water Depth in Test Well
Banning Strand of San Andreas Fault
Unmapped Fault
1500 m/s Velocity Contour (Probable Water Level)
Water Level
Distance (m) From South
VE: ~2:1

Figure 27a

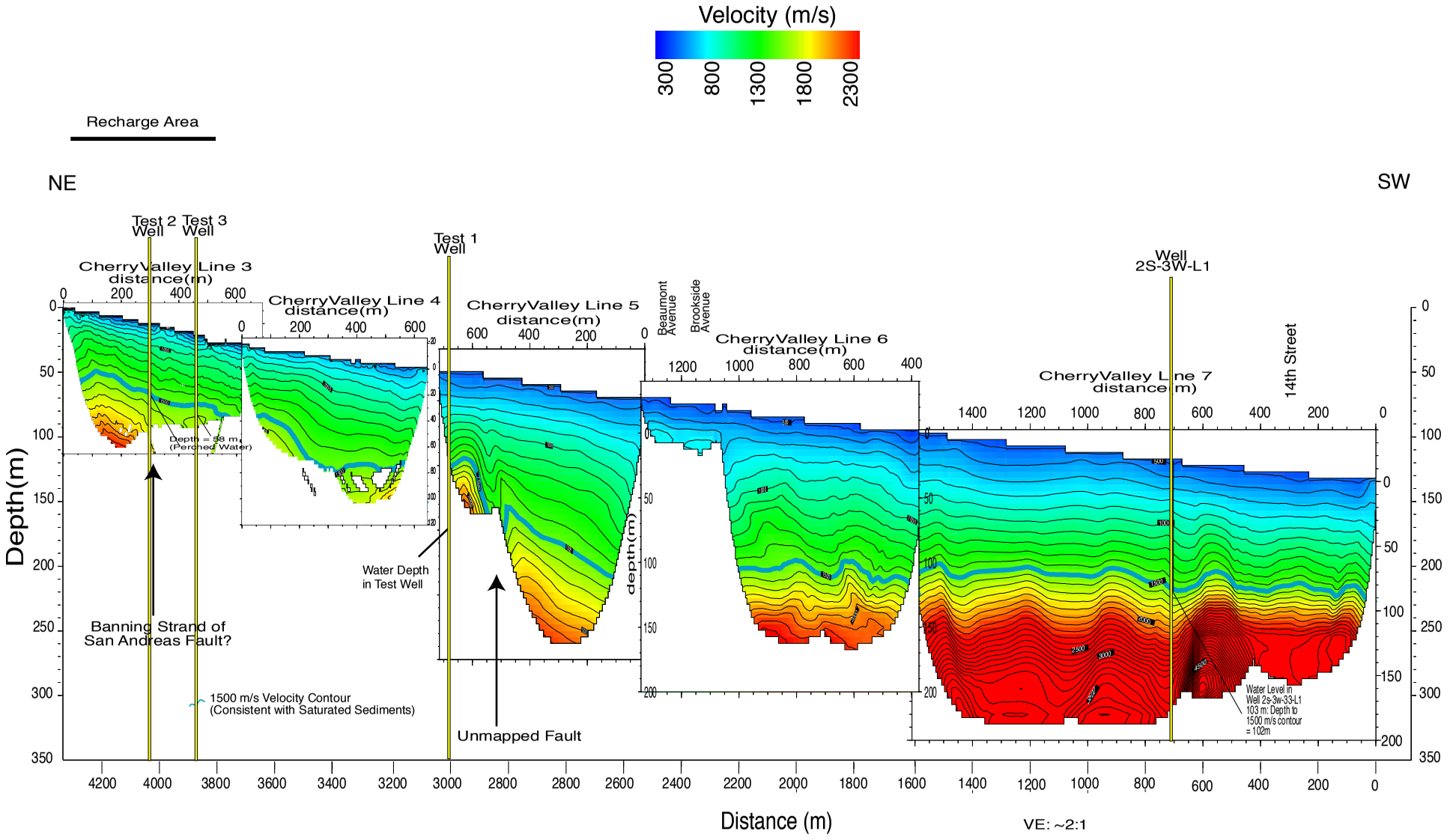
Velocity (m/s)
300
800
1300
1800
2300
Recharge Area
NE
SW
Test 2 Well
Test 3 Well
Test 1 Well
Well 2S-3W-L1
CherryValley Line 3 distance(m)
CherryValley Line 4 distance(m)
CherryValley Line 5 distance(m)
CherryValley Line 6 distance(m)
CherryValley Line 7 distance(m)
Beaumont Avenue
Brookside Avenue
14th Street
Depth = 38 m (Perched Water)
Water Depth in Test Well
Banning Strand of San Andreas Fault?
1500 m/s Velocity Contour (Consistent with Saturated Sediments)
Unmapped Fault
Water Level in Well 2s-3w-33-L1 103 m: Depth to 1500 m/s contour = 102m
Depth(m)
Distance (m)
VE: ~2:1

Figure 27b

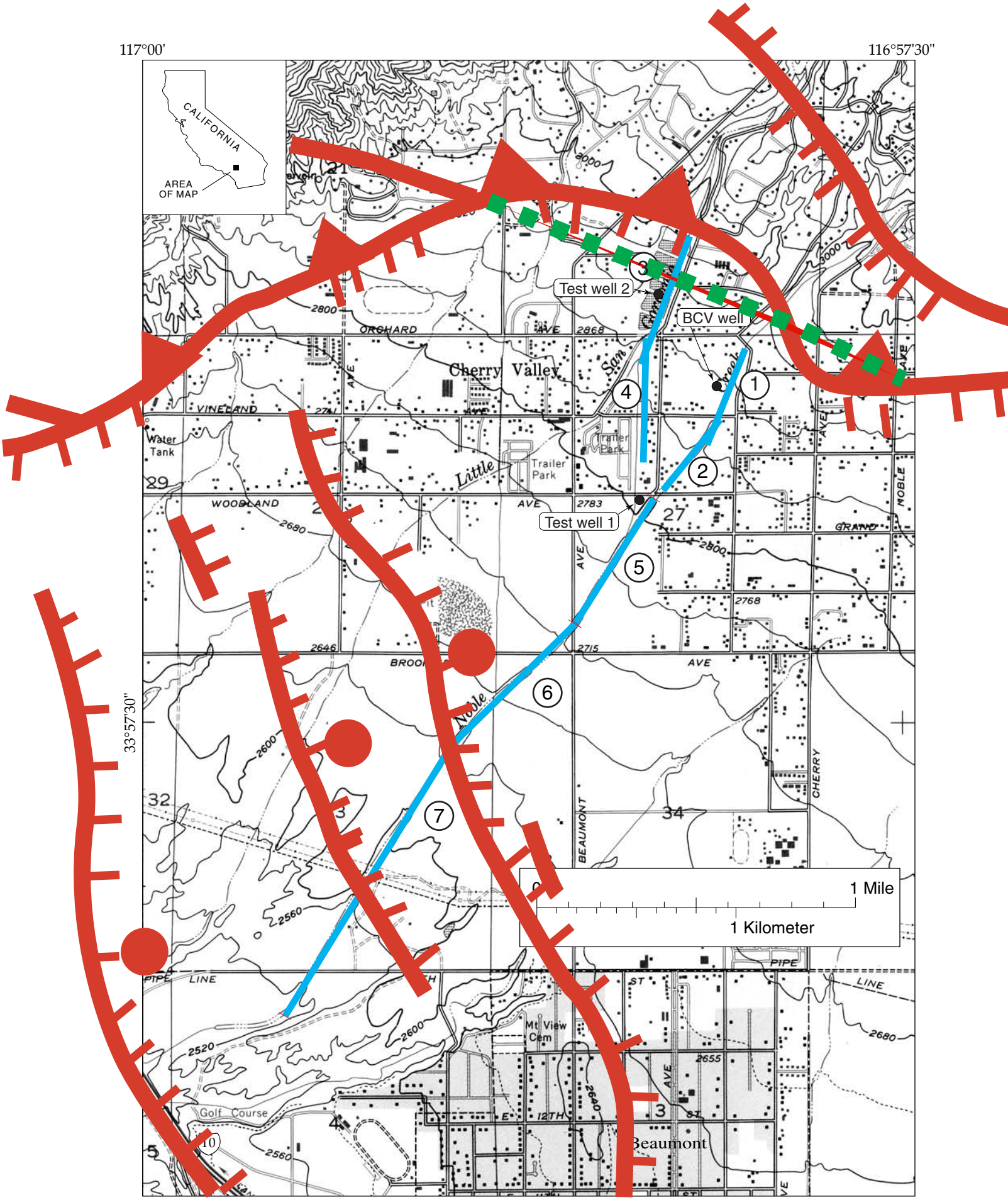
117°00'
116°57'30"
33°57'30"
CALIFORNIA
AREA OF MAP
Test well 2
BCV well
Test well 1
Cherry Valley
Sam Creek
Little Trailer Park
Noble Creek
Water Tank
Mt View Cem
Golf Course
Beaumont
ORCHARD
VINELAND
WOODLAND
BROOK
AVE
BEAUMONT
CHERRY
NOBLE
GRAND
PIPE LINE
12TH ST
1 Mile
1 Kilometer

Figure 28